A Study of $t\bar{t}$ system in Muon+Jets channel at $\sqrt{s}$ = 7 TeV at CMS

By

Muhammad Gul

Department of Physics
Quaid-I-Azam University
Islamabad 45320, Pakistan

January 25, 2013

CERN-THESIS-2013-184
25/05/2013

This work is submitted as a dissertation
in partial fulfillment of
the requirement for the degree of

MASTER OF PHILOSOPHY
in
PHYSICS

Department of Physics Quaid-I-Azam University
Islamabad 45320
Pakistan

Certificate

It is hereby certified that the research work presented in this thesis entitled "*A Study of $t\bar{t}$ system in Muon+Jets channel at $\sqrt{s}$ = 7 TeV at CMS*" by **Mr. Muhammad Gul** for the degree of Master of Philosophy was carried out and completed under my supervision.

Prof. Dr. Hafeez R. Hoorani
Supervisor
National Centre for Physics
Quaid-I-Azam University Campus
Islamabad 45320

Submitted through:

Prof. Dr. Muhammad Zakaullah
Chairman
Department of Physics
Quaid-I-Azam University
Islamabad 45320

Quaid-I-Azam University

Date: **January 25, 2013**

Author: Muhammad Gul

Title: A Study of $t\bar{t}$ system in Muon+Jets channel at $\sqrt{s}$ = 7 TeV at CMS

Department: Physics

Degree: MPhil

Permission is herewith granted to Quaid-I-Azam University to circulate and to have copied for non-commercial purposes, as its discretion, the above title upon the request of individuals or institutions.

_____

Signature of Author

To my family

Acknowledgement

I would like to give my special thanks to my thesis advisor, Professor Hafeez Hoorani, for all the patience, kindness and wisdom he has given to me. Professor Hafeez Hoorani is the person who opened the door of high energy physics to me. He guided me through the whole analysis. Without his help, I can't finish this program by now. I would also like to acknowledge his assistance in reading and correcting this thesis.

Thanks to all the members in High Energy Physics group at the National Center for Physics (NCP), especially Dr. M. Irfan Asghar, Taimoor Khurshid, Izhar Sagheer and Qamarul Hasan for their positive criticism and continuous support through the early stages of chaos and confusion. Thanks to Dr. Ashfaq Ahmad, Dr. Shamoona Fawad, Dr. Jamila Bashir Butt, M. Ahmad, Qasim Ali, Waqar, Sobia Khanum, Tahira Najeeb, M. Bilal Kiani, Mehar Ali Shah, Shoiab Khalid, M. Shoiab, Shawana Hameed, Fakhra Ghafoor and Nazir Ahmad who helped me in completing this thesis.

My very special thanks go to Wajid Ali Khan who gave me full support during my analysis and writing this thesis. I have a lot of respect for his wisdom of dealing with difficult situations, e.g. when we were under a lot of pressure to do synchronization. All the discussions with him and his suggestions are invaluable aid for me.

I am very grateful to Muhammad Islam, Nasir Ali, Sherin Jan, M. Rahim, M. Sahil, M. Zia, M. Ibrahim, M. Afzal, Anas Gul, Sardar Badshah, Rizwan Maqsood, Gul Mir, Waqas Kiani, M. Hayat, Tanveer Ahmad and Sahib Noor for their support to complete my work.

The greatest thanks go to my parents who encouraged me when I faced difficulties. Finally, I am grateful to my wife and sons, Muhammad Sudais and Muhammad Shuraim. They are always the source of my happiness and encourage me when I was depressed.

Muhammad Gul

Abstract

The top quark was discovered by the CDF and DØ experiments at Fermilab in 1995. It is the weak isospin doublet of bottom quark and the most massive of known elementary particles. The top quark produced primarily by the strong interaction but can only decay through the weak force. Top quark is produced in pair or in single state. At LHC $t\bar{t}$ production is 90% through gluon fusion and 10% through quark annihilation. At designed luminosity of LHC, eight million events of $t\bar{t}$ pairs will be produced per year.
The kinematic characteristics of events are studied with exactly one isolated muon in association with hard jets and exhibiting substantial missing transverse energy.
The analysis is based on $\int \mathcal{L}\, dt = 0.959\ fb^{-1}$ data (run number 165088-167913) collected by CMS experiment in 2011. Based on synchronization, data is processed and compare with MC for different $t\bar{t}$ parameters.

Table of Contents

Table of Contents i

1 Introduction 1

2 LHC at CERN 8
- 2.1 Detectors at LHC . . . 8
- 2.2 The CMS Detector . . . 9
  - 2.2.1 The Tracker . . . 10
  - 2.2.2 The Electromagnetic Calorimeter (ECAL) . . . 11
  - 2.2.3 The Hadronic Calorimeter (HCAL) . . . 12
  - 2.2.4 Magnet System . . . 13
  - 2.2.5 The Muon System . . . 14
- 2.3 Pseudorapidity . . . 15
- 2.4 The Beam Spot . . . 15
- 2.5 The Trigger System in CMS . . . 15
- 2.6 CMS Analysis Framework . . . 16
- 2.7 Event Generators . . . 17
  - 2.7.1 POWHEG . . . 18
  - 2.7.2 MadGraph . . . 18
- 2.8 Particle Flow (PF) Algorithm . . . 18
- 2.9 B-tagging . . . 18
  - 2.9.1 B-tagging observables . . . 19
  - 2.9.2 B-tag algorithm . . . 19
- 2.10 Event Shape Variables . . . 19
  - 2.10.1 Sphericity . . . 19
  - 2.10.2 Aplanarity . . . 20
  - 2.10.3 Circularity . . . 20
- 2.11 Pile-up . . . 20
- 2.12 CMS active status report 2012 . . . 21

3 Data Sets and Event Selection 22
- 3.1 Monte Carlo Background Samples . . . 22
- 3.2 MC samples . . . 23
- 3.3 Event Selection . . . 24
- 3.4 Synchronization . . . 26
  - 3.4.1 Synchronization for signal MC . . . 27

3.4.2 Synchronization for W+Jets MC . . . 27
3.4.3 Synchronization for Data . . . 27
3.5 Luminosity . . . 29
3.6 HDECAY . . . 30
3.7 A real $t\bar{t}$ event . . . 31

4 Results and Discussion **32**
4.1 Work Summary . . . 32
4.2 Plots description . . . 32
4.2.1 Kinematic distribution of inclusive jets . . . 33
4.2.2 Distribution of four leading jets pT . . . 34
4.2.3 Pseudorapidity distribution of leading jets . . . 35
4.2.4 Mass distribution of leading jets . . . 36
4.2.5 Phi distribution of leading jets . . . 37
4.2.6 Kinematics distributions of non b-jets . . . 38
4.2.7 Kinematics distributions of b-jets . . . 39
4.2.8 Combined Secondary Vertex (CSV) distribution . . . 40
4.2.9 Hadronic W boson . . . 41
4.2.10 Hadronic Top quark . . . 42
4.2.11 Muon kinematics . . . 44
4.2.12 Missing Transverse Energy (MET) . . . 45
4.2.13 Kinematics of leptonic W boson . . . 46
4.2.14 Leptonic Top quark . . . 47

Conclusion **50**

Bibliography **51**

List of Figures

1.1 Standard Model of Particle Physics. 2
1.2 The production of $t\bar{t}$ and single top. 4
1.3 Decay of $t\bar{t}$ and single top. (a) shows hadronic decay of $t\bar{t}$, (b) semileptonic decay of $t\bar{t}$, (c) leptonic decay and (d) the decay of single top. 6
1.4 Production of SM Higgs from gg fusion. (a) the Higgs production through top quark loop (b) the associative Higgs production with $t\bar{t}$. 7

2.1 The Large Hadron Collider. 9
2.2 Complete picture of CMS. 10
2.3 The tracker layout in the 1^{st} quadrant with endcap and barrel regions. . . . 11
2.4 CMS ECAL layout. 12
2.5 The HCAL in CMS. 13
2.6 Muon System in endcap and barrel regions in CMS. 14
2.7 Pseudorapidity Values in 1^{st} Quadrant. 15
2.8 Pile-up Events. 21
2.9 A comparison of efficiency of CMS detectors from 2010 to 2012. 21

3.1 SM backgrounds to $t\bar{t}$ semiletonic decay. 24
3.2 Shows a real $t\bar{t}$ event in 2011 data. 31

4.1 Distributions of all jets in pp collision. (a): pseudorapidity (η) of jets. (b): mass of jets. (c): distribution of azimuthal angle (ϕ) of jets. (d): transverse momentum (pT) of jets. 33
4.2 Distributions of transverse momentum (pT) of four leading jets (highest transverse momentum jets). (a): pT of leading jet. (b): pT of 2^{nd} jet. (c): pT of 3^{rd} jet. (d): pT of 4^{th} jet. 34
4.3 Distribution of pseudorapidity (η) of four leading jets (highest transverse momentum jets). (a): η of leading jet. (b): η of 2^{nd} jet. (c): η 3^{rd} jet. (d): η of 4^{th} jet. 35

4.4 Mass distributions of four leading jets (highest transverse momentum jets). (a): mass of leading jet. (b): mass of 2^{nd} jet. (c): mass 3^{rd} jet. (d): mass of 4^{th} jet. 36
4.5 Distributions of azimuthal angle (ϕ) of four leading jets (highest transverse momentum jets). (a): phi of leading jet. (b): phi of 2^{nd} jet. (c): phi 3^{rd} jet. (d): phi of 4^{th} jet. 37
4.6 Distribution of non b-jets in $t\bar{t}$ decay. (a): transverse momentum of leading non b-jet. (b): transverse momentum of 2^{nd} non b-jet. (c): pseudorapidity (η) of leading non b-jet. (d): pseudorapidity (η) of 2^{nd} non b-jet. 38
4.7 Distribution of b-jets. (a): transverse momentum of leading b-jet. (b): transverse momentum of 2^{nd} b-jet. (c): pseudorapidity (η) of leading b-jet. (d): pseudorapidity (η) of 2^{nd} b-jet. 39
4.8 (a): phi (ϕ) distribution of leading b-jet. (b): phi (ϕ) distribution of 2^{nd} b-jet. (c): combined secondary vertex (CSV) discriminator used for b-tagging. (d): track counting high efficiency (TCHE) b-jet discriminator. . 40
4.9 Distribution of W boson parameters reconstructed from two non b-jets. (a): transverse momentum (pT). (b): pseudorapidity (η). (c): azimuthal angle (ϕ). (d): mass of W boson. 41
4.10 Distribution of hadronic top quark reconstructed from hadronic W boson and b-jet. (a): transverse momentum (pT). (b): pseudorapidity (η). (c): azimuthal angle (ϕ). (d): mass of top quark. 42
4.11 Distribution of hadronic top quark reconstructed from hadronic W boson and b-jet. (a): x-component of momentum. (b): y-component of momentum. (c): z-component of momentum. (d): the transverse energy. . 43
4.12 (a): Transverse momentum of the selected muon. (b): pseudorapidity (η) of the selected muon. (c): phi (ϕ) distribution of the selected muon. (d): track counting high purity b-tagging (TCHPbT) discriminator. 44
4.13 (a): Missing transverse energy (MET) distribution. (b): phi distribution of MET. (c): photon isolation. (d): opening angle between muon and MET. 45
4.14 Distribution of W boson (leptonic W boson) constructed from muon and missing transverse energy (MET). (a): the pseudorapidity. (b): mass of W boson. (c): the transverse energy. (d): the transverse mass. 46
4.15 Distribution of top quark reconstructed from the leptonic W boson and b-jet (leptonic top quark). (a): the pseudorapidity. (b): the mass of leptonic top quark. (c): the phi distribution. (d): the transverse momentum. 47

4.16 Distribution of top quark reconstructed from the leptonic W boson and b-jet (leptonic top quark). (a): the transverse energy. (b): transverse mass. (c): x component of momentum (d): y component of momentum. 48
4.17 Distribution of leptonic top quark. (a): the z component of momentum. (b): x component in space. (c): y component in space. (d): z component in space. 49

List of Tables

3.1 Monte Carlo samples with cross sections, luminosity and the perturbative order of calculations. 23
3.2 Data set used in this analysis, the range of run numbers, corresponding luminosity and JSON file. 23
3.3 The selection cuts applied on different objects of $t\bar{t}$ semileptonic decay. . . 26
3.4 Remarks of different groups for synchronization done in table 3.5. 27
3.5 Synchronization of different groups for $t\bar{t}$ muon+jets channel. 28
3.6 Synchronization for W+Jets of different groups. Our results (NCP) are matching well at different levels of cut flow. 29
3.7 Synchronization for Data of different groups. Our results (NCP) are matching well. 29
3.8 Luminosity calculated for data 2011A. 30
3.9 Branching ratios (BR) and decay width of top quark. It has been calculated using HDECAY program. 30

Chapter 1

Introduction

Particle physics addresses the question, "what are the constituents of matter?" on the most fundamental level–which is to say, on the smallest scale of size. Matter consists of atoms which further composed of subatomic particles such as electrons, protons etc, with vast empty spaces in between. Our visible universe is made of protons, electrons, or one could say from the first family of the Standard Model (SM), that is electrons and quarks [1].

The Standard Model (SM) of Particle Physics

SM is the current and compact model of particle physics. Reduction principle provides a simple way to make a compact picture of variety of macroscopic forms of matter in terms of few microscopic constituents, interact by a small number of fundamental forces. SM is experimentally verified model in many respects and all of its building blocks have been experimentally established so far. In particular, the Higgs boson which is recently discovered by the CMS and ATLAS require more data to verify its predicted properties [2].

The Standard Model (SM) has three main components:

1. The basic constituents of matter are leptons and quarks which are realized in three families of identical structure. The entire ensemble of these constituents has been found experimentally.

2. There are four forces act between the leptons and quarks, the strong, electromagnetic (EM), weak and gravitational. The electromagnetic and weak forces are unified in the Standard Model called the electroweak force. The fields associated with the strong, weak as well as with the electromagnetic force, are spin-1 fields, describing by the gluons g, the electroweak gauge bosons $W^{\pm}$ and Z and the photon γ respectively. The gravitational interaction is mediated by a spin-2 field, describing by the graviton G, which is quite different from spin-1 gauge fields and therefore not included in the Standard Model.

3. The third component known as the corner stone of the SM is the Higgs mechanism. All the fundamental particles acquire masses through this mechanism. The picture is correct because CMS and ATLAS announced the existence of Higgs like particle.
The story will not end when the Higgs boson find with all of its predicted properties, because particle theory needs a universal theory that explains the whole phenomena of the subject. The two interactions, electromagnetic and weak are unified; the next step is to include strong interaction.

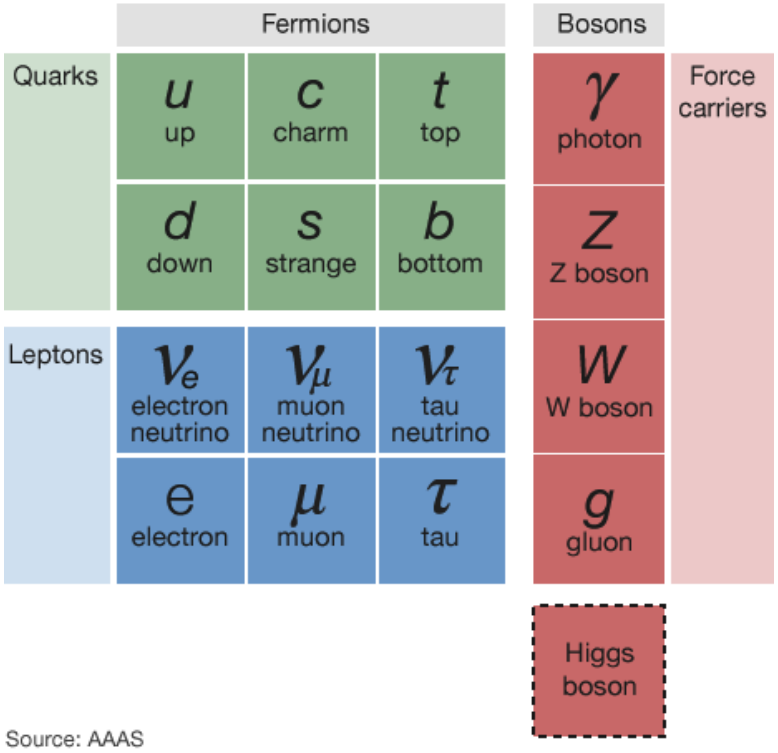

Figure 1.1: Standard Model of Particle Physics.

The Electromagnetic (EM) Force

EM force is responsible for the attraction or repulsion of charged bodies. Its magnitude is directly proportional to the product of their charges and inversely proportional to the square of distance between them. Electromagnetic field is produced by a charged particle when it is in motion. This concept was presented by Faraday and Maxwell. It is responsible for the binding of atoms. The interatomic and intermolecular forces are all electrical in nature and mainly govern all known phenomena. The mediator of this force is photon γ. It is a long range force and its strength is determined by the dimensionless

number $\alpha = 1/137$ known as the fine structure constant [3]. The phenomenology of the Electromagnetic Force is described by Quantum Electrodynamics or QED.

The Strong Force

This force is responsible for the binding of protons and neutrons in a nucleus. It also holds quarks together to form protons, neutrons and other hadrons. It is a short range force effective over the nuclear dimension $\sim O(10^{-15}\text{m})$. Its relative strength is 1. At atomic scale it is about 100 times stronger than the electromagnetic force. The mediator of this force is gluon [4]. The phenomenology of the strong force is described by Quantum Chromodynamics (QCD).

The Weak Force

Weak force is responsible for the radioactive decay of subatomic particles and initiates the process known as hydrogen fusion in stars. According to the Standard Model of particle physics the weak interaction is mediated by $W^{\pm}$ and Z bosons [5]. Beta decay is the best known effect of weak interaction. The mediators are much heavier than protons or neutrons and it is the heaviness that accounts for the very short range of the weak interaction. It is effective over a distance of order of 10^{-16} cm. Quark flavor changing is a property of Weak Interaction. It is the only interaction which violates parity-symmetry. It also violates CP symmetry [6].

The Top Quark

Amongst all known elementary particles, the top quark is special one: weighing as much as a Tungsten atom, it completes the so-called 3^{rd} generation of quarks and is the only quark whose properties can be directly measured. It decays mostly to a W boson and a bottom (b) quark, and can therefore be identified from final states which involve the complete usage of the CMS detector; muons, electrons, jets, missing transverse energy, almost all particles or experimental signatures one can think of may be produced in top-quark events. Many of the top quark's fundamental properties were studied in detail by the collaborations of CDF and DØ, at energies up to the threshold of the Tevatron accelerator at Fermilab [7, 8]. Top is the weak isospin partner of the bottom quark. Like the up and charm quarks, it has electric charge of +2/3 and a spin of +1/2. The top's most remarkable property, unique amongst the quarks is its large mass measured to be 172.5±1.1 GeV/c^2 [9]. This is a mass-energy nearly 37 times greater than the next-to-most massive quark, the bottom quark (whose mass is measured to be $4.67 \pm 0.18 \pm 0.06$

GeV/c^2) [10]. As a result of this high mass, the top exhibits several properties which the less massive quarks do not. One resultant experimental consequence is that the top has an extremely short lifetime about 4×10^{-25} s, according to the Standard Model [11]. Its large mass has inspired numerous theoretical models in which the top quark plays a special role in the generation of mass or in the physics of new, undiscovered particles. The top quark often acts as either a direct contributor to new physics or an important background in new-particle searches in these models [12].

Top Quark Production

At hadrons colliders two distinct SM production mechanisms are possible: dominant $t\bar{t}$ production, via the strong interaction; single top quark can be produced through charged-current electroweak interactions. $t\bar{t}$ production occurs via two main processes: either by gluon fusion $gg \rightarrow t\bar{t}$ or by quark anti-quark annihilation $q\bar{q} \rightarrow t\bar{t}$. The gluon fusion process is dominant at LHC which is about 90% and $q\bar{q}$ is 10%. At Tevatron these percentages are other way round. Due to the large top-quark mass, these processes are well suited to test the predictions of the standard model (SM) of particle physics and to search for new phenomena. Measurements of the single top-quark production cross section also provide an unbiased determination of the magnitude of the Cabibbo-Kobayashi-Maskawa (CKM) matrix element V_{tb} [13].

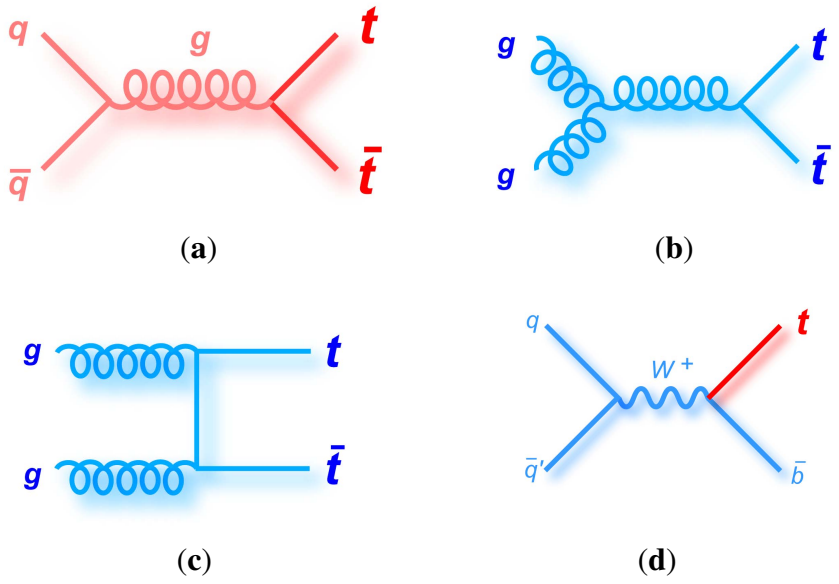

Figure 1.2: The production of $t\bar{t}$ and single top.

Top Quark Decays

The SM predicts $B(t \to bW) > 0.998$. Other decays allowed in the SM are not only rare, but also mostly too difficult to disentangle from backgrounds to be observed in the foreseeable future [14]. W boson can decay into $q\bar{q}$ or lepton and corresponding neutrino. Depending on the W decay $t\bar{t}$ can decay in three modes:

- **Hadronically**
  The largest fraction (46.2%) of $t\bar{t}$ pair decays where both $W^{\pm}$ bosons decay hadronically. The decay can be written as $t\bar{t} \to b\bar{b}W^+W^- \to b\bar{b}q\bar{q}q\bar{q}$. This channel has the combined advantage of being the most probable decay mode with (at least in principle) completely measurable particles in the final state. The solely hadronic activity imposes large challenges, especially at a hadron collider. Effective selection will be a challenging task due to the large hadronic backgrounds [15].

- **Semileptonically**
  The second largest fraction (43.5%) of final states for $t\bar{t}$ pair decay originates from a combination of one hadronic and one leptonic W boson decay. These decays can be written as $t\bar{t} \to b\bar{b}W^+W^- \to b\bar{b}q\bar{q}l\nu$ where l is one of the lepton and ν is the corresponding neutrino [16].

- **Leptonically**
  The remaining (10.3%) decay mode occurs when both W bosons decay leptonically, producing a pair of a oppositely charged leptons and two neutrinos. This can be written as $t\bar{t} \to b\bar{b}W^+W^- \to b\bar{b}l\bar{l}\nu\bar{\nu}$. Dileptonic decays are intrinsically underdetermined, due to the undetectable two neutrinos. The problem is more pronounced if one or both charged leptons are a tau, as described for the semileptonic decay mode. Good measurement of the leptons therefore demands again the rejection of taus in the final state [17].

The Higgs boson

On July 04, 2012 during a seminar at CERN Peter Higgs said to the audience. “He was among a half-dozen physicists who in the 1960s proposed what is now known as the Higgs mechanism, hypothesizing the existence of a field permeating all of space, along with an associated particle. The field imparts particles with mass by exerting a sort of drag on them, slowing them down much like a human being slows down when she tries to walk through water instead of air” [18]. At the same day LHC’s detector CMS and ATLAS announced that they have found a new particle with a mass near to 125

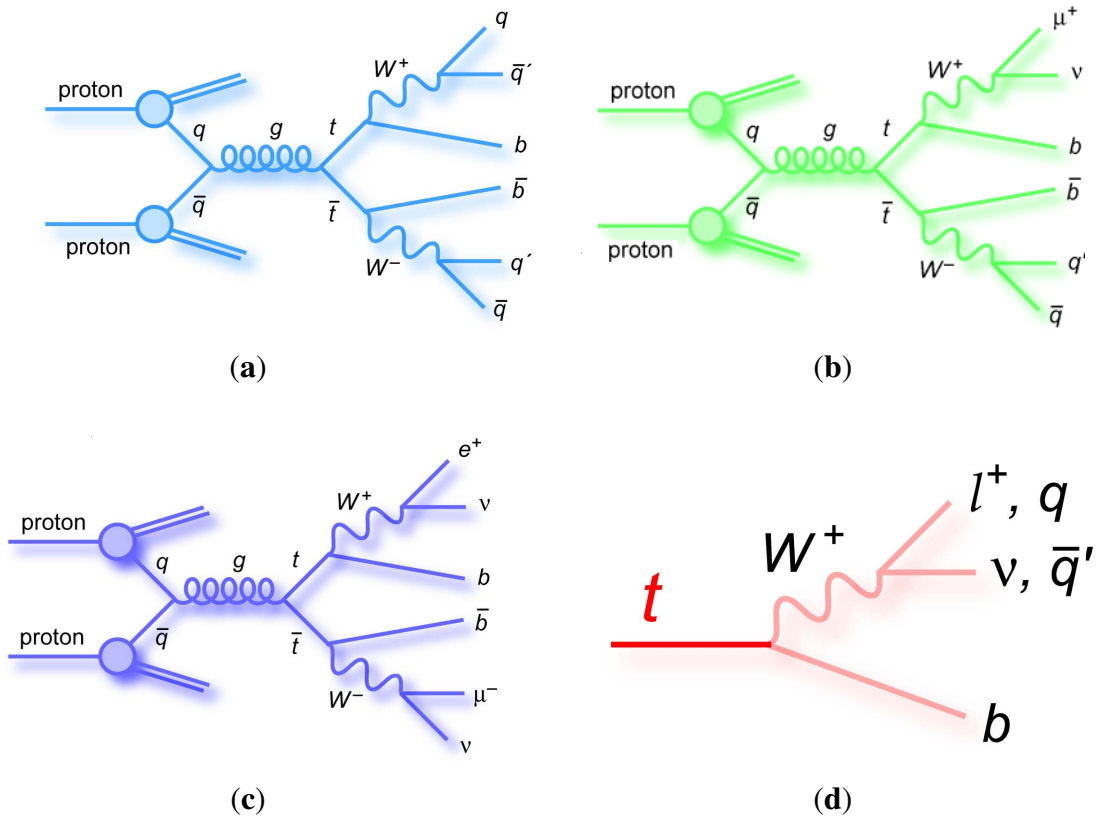

Figure 1.3: Decay of $t\bar{t}$ and single top. (*a*) shows hadronic decay of $t\bar{t}$, (*b*) semileptonic decay of $t\bar{t}$, (*c*) leptonic decay and (*d*) the decay of single top.

GeV [19, 20]. The newly found particle fits the bill for the Higgs boson, but researchers cautioned that more work is needed to compare the properties of the particle to those predicted for the Higgs. After all, the LHC's detectors cannot identify the Higgs directly. So it is too early to decide whether it is SM Higgs or not.

Top Quark and the Higgs boson

Higgs coupling to fermions is proportional to their mass m_f:

$$g_{Hf\bar{f}} = \frac{m_f}{v}$$

Since Top quark is the heaviest among all the fundamental particles, so it is important in the Higgs searches. At LHC the dominant process for the Higgs production is gluon fusion (gg $\rightarrow$ H) [21]. The massless gluons are coupled to Higgs through top quark loop due to the strong Higgs to top quark Yukawa coupling. Feynman diagrams for these

processes are shown in Fig. 1.4. Thus good knowledge about the top quark is crucial for the calculation of the Higgs production cross section.

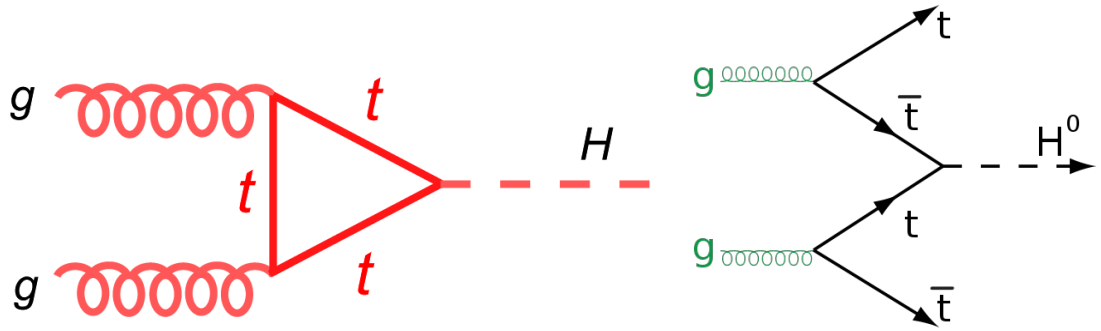

(**a**) (**b**)

Figure 1.4: Production of SM Higgs from gg fusion. (*a*) the Higgs production through top quark loop (*b*) the associative Higgs production with $t\bar{t}$.

Chapter 2

LHC at CERN

The Large Hadron Collider (LHC) is the world's largest and highest-energy particle accelerator. It is built by the European Organization for Nuclear Research (CERN) from 1998 to 2008. Its aim is to test the predictions of different theories of high-energy physics, particularly the existence of the Higgs boson and the large family of new particles predicted by theory (supersymmetry). The LHC lies in a tunnel 27 km in circumference, about 100 m beneath the Franco-Swiss border near Geneva, Switzerland. It is designed to collide particle beams (lead ions or protons) traveling in opposite direction inside the circular accelerator, gaining energy with every lap. On November 20, 2009 LHC was successfully run and three days later proton–proton collisions took place at the injection energy of 450 GeV per beam. On March 30, 2010, the first collision took place between two beams at 7 TeV centre of mass energy, setting the current world record for the highest-energy man-made particle collisions, and the LHC began its research program [22].

2.1 Detectors at LHC

Six detectors have been constructed at the LHC, at different intersection points. Two of them, the ATLAS (A Toroidal LHC Apparatus) experiment and the Compact Muon Solenoid (CMS), are general purpose particle detectors. ALICE (A Large Ion Collider Experiment) and LHCb (Large Hadron beauty), have more specific roles and the last two, TOTEM (Total Elastic and diffractive cross section Measurement) and LHCf (Large Hadron Collider forward), are very much smaller and are for specific research. A short summary of the main detectors is given below [23]:

- CMS: Search for the Higgs boson and look for clues to the nature of dark matter are the main purposes of this detector.

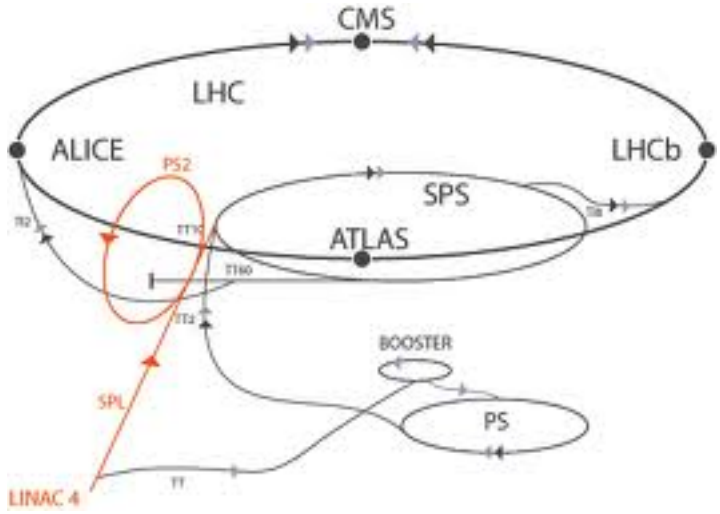

Figure 2.1: The Large Hadron Collider.

- ATLAS: It will be used to look for signs of new physics, including the extra dimensions and origins of mass.
- ALICE: The detector is made to study quark–gluon plasma that existed shortly after the Big Bang.
- LHCb: In the Big Bang equal amounts of matter and antimatter were produced. LHCb will try investigate what happened to the "missing" antimatter.

2.2 The CMS Detector

Compact Muon Solenoid (CMS) name represents three main features of the detector. Compact is due to its small size comparing to its huge weight, muon is one of the particles detected by it and solenoid is used for the coil inside its gigantic superconducting magnet. The CMS detector is 15m wide, 21 m long and 15m high. It is a general-purpose detector, used to study many aspects of proton collisions at the center-of-mass energy (14 TeV) of the LHC particle accelerator. CMS is made in layers of concentric cylinders which are designed to measure the energy and momentum of electrons, photons, muons, and other products of the collisions. The main distinguishing properties of CMS are a high-field solenoid, a homogeneous scintillating-crystals-based ECAL (electromagnetic calorimeter) and a full-silicon-based inner tracking system. The coordinate system chosen by CMS has the origin centered at the collision point inside the detector, the y-axis pointing vertically upward and the x-axis pointing radially towards the center of LHC. Thus, the z-axis points along the beam direction. The azimuthal angle ϕ is measured in

the x-y plane from the x-axis. The radial coordinate in x-y plane is denoted by r. From the z-axis the polar angle θ is measured [24].

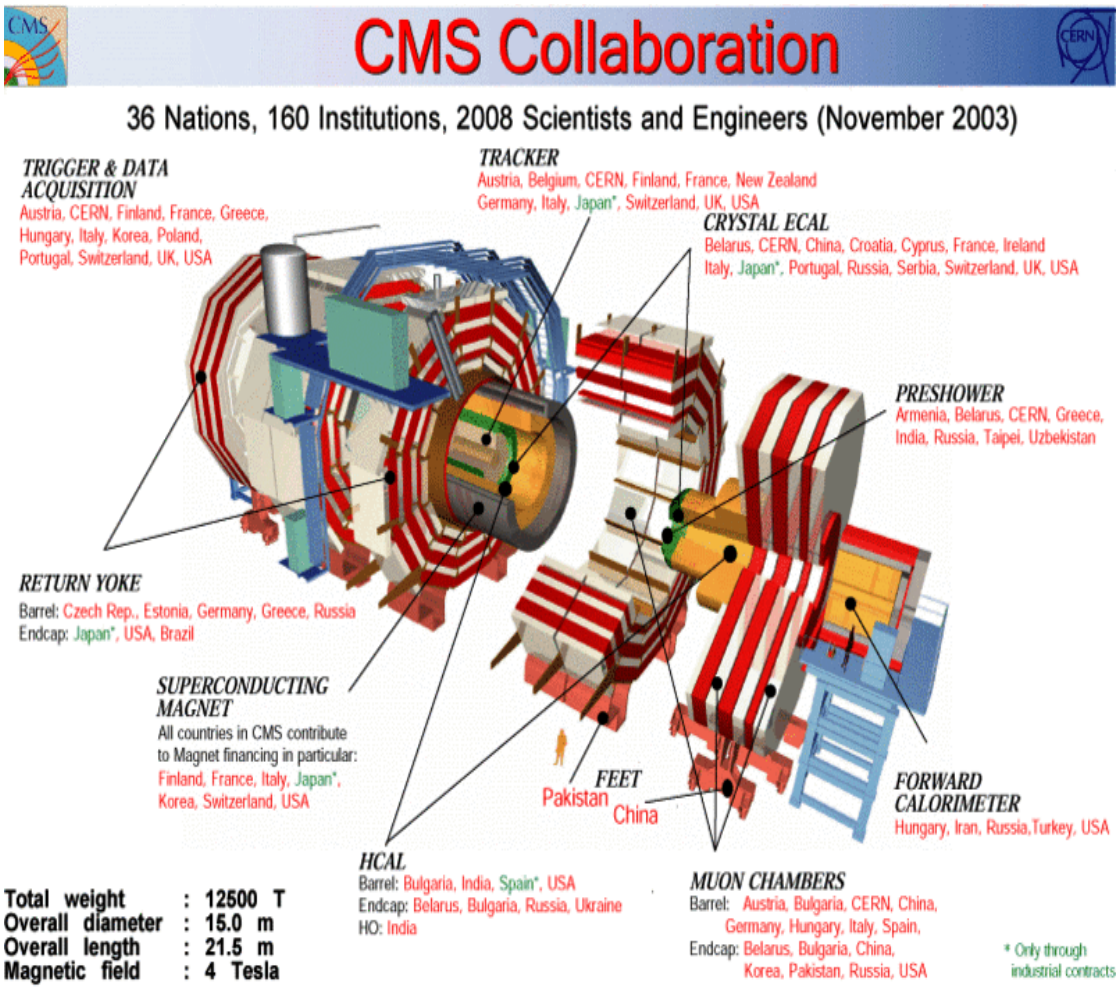

Figure 2.2: Complete picture of CMS.

2.2.1 The Tracker

The momentum of a charge particle is measured from its track inside the magnetic field. It is an important parameter to build up a picture of events at the heart of the collision. In CMS the inner tracker serves to identify the tracks of individual particles immediately around the beam spot. These tracks are then matched to the vertices from which they originated [25]. The tracker needs to record particle paths accurately and in the mean time should be lightweight so as to disturb the particle as little as possible. Tracker does this by taking position measurements so accurate that tracks can be reliably reconstructed just using a few measurement points. Tracker is the inner most layer of the detector, hence receives the largest number of particles produced. At the LHC design luminosity of 10^{34}

cm^{-2} s^{-1} there will be on average about 1000 particles from more than 20 overlapping proton-proton interactions traversing the tracker for every 25 ns [26]. So it is necessary to choose the construction materials carefully to resist radiation.

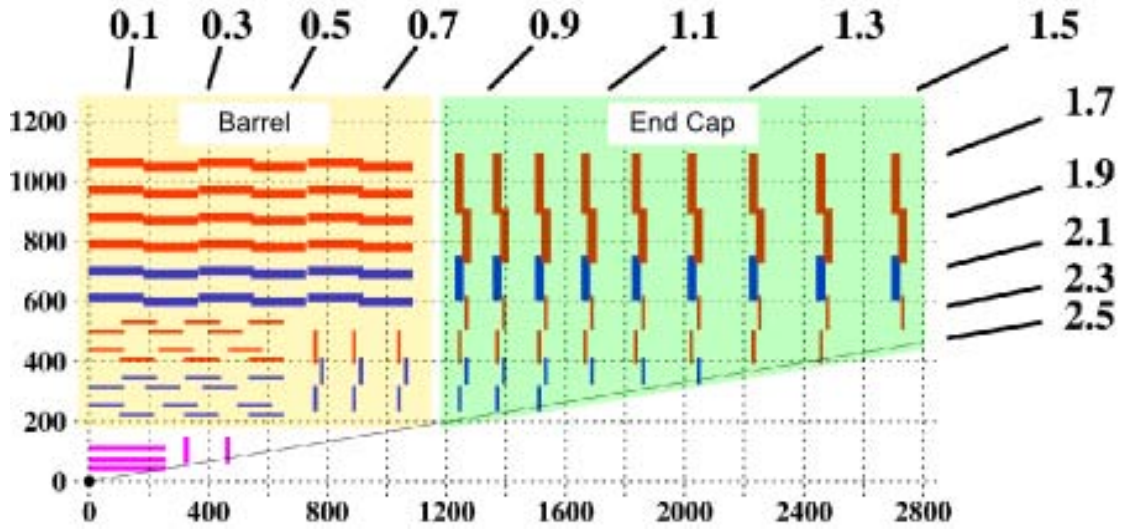

Figure 2.3: The tracker layout in the 1^{st} quadrant with endcap and barrel regions.

2.2.2 The Electromagnetic Calorimeter (ECAL)

The ECAL is installed between the tracker and Hadronic Calorimeter (HCAL) to measure with high accuracy the energies of electrons and photons. It consists of three partitions: Barrel, Endcaps and Preshower. The ECAL barrel (EB) begins at a radius of 129 cm and covers the range $|\eta| < 1.4442$ [27]. The ECAL endcaps (EE) are located 314 cm from the vertex and cover the range $1.56 < |\eta| < 3.0$. Preshower detector (PS) has two planes of lead absorber (Pb-Si), followed by silicon strip detectors, which is placed in the endcaps, covering $1.65 < |\eta| < 2.5$. Lead tungstate, $PbWO_4$ has been chosen as the active medium for the CMS electromagnetic calorimeter (ECAL) [28]. It is an extremely dense but optically clear material, efficient for stopping high energy particles. It has short radiation lengths (X_0 = 0.89 cm) and are fast that is 80 percent of light is emitted within 25 ns. $PbWO_4$ crystal is the first element that converts energy into light. A photodetector is used to convert light into photocurrent. A preamplifier is used to amplify the photocurrent. It is then converted into a voltage waveform. The signal is then acquired and digitized. The resulting data is transported through optical fiber to the upper-level readout. It is a homogeneous calorimeter; designed in such a way to give the highest possible energy resolution in a very severe radiation environment.

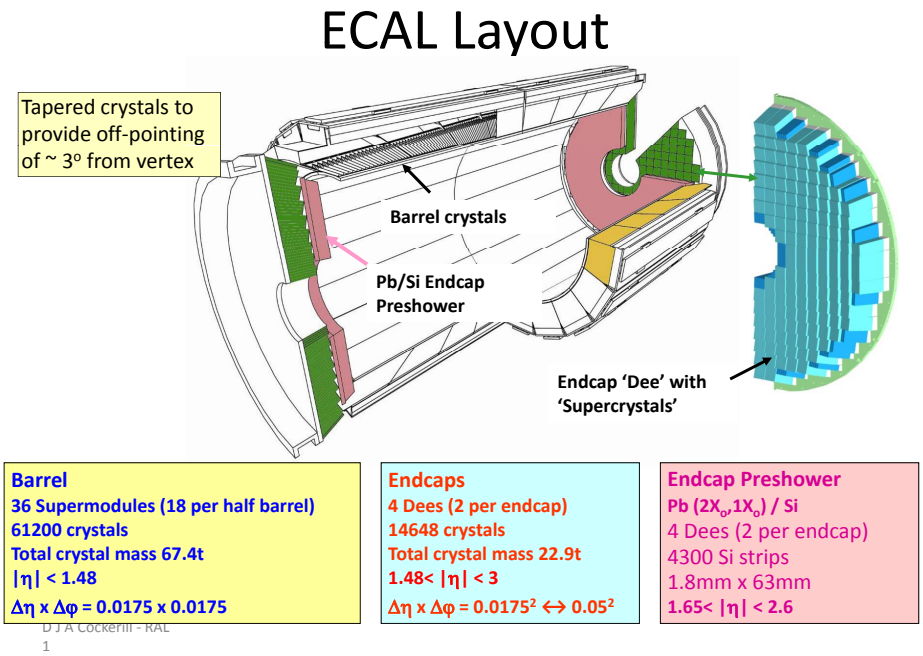

Figure 2.4: CMS ECAL layout.

2.2.3 The Hadronic Calorimeter (HCAL)

The HCAL plays an essential role in the measurement of the energy of quarks and gluons by absorbing jets of particles the quarks and gluons hadronize into. It is comprised of four subdetectors, a barrel detector (HB) covering $|\eta| < 1.3$, two endcap detectors (HE) covering $1.3 < |\eta| < 3.0$, two forward detectors (HF) covering $2.8 < |\eta| < 5.0$, and a detector outside of the solenoid (HO) covering $|\eta| < 1.3$ [29]. The hadronic calorimeter barrel (HB) is 860 cm long, inner radius is 177 cm and outer radius is 295 cm. It is divided into two half-barrel HB+ and HB- covering the positive and the negative z axis parts respectively. Each of them contains 18 identical wedges constructed of flat brass absorber plates aligned parallel to the beam axis. The HE covers 34% of the solid angle in the η range; located from $|z| = 388$ cm to $|z| = 570$ cm, with thickness corresponding to 10 interaction lengths. The HO is placed outside the solenoid serving as additional absorbing material. The HF is a very forward detector placed at $|z| = 11.2$ m. It is made of a cylindrical steel structure with inner radius 12.5 cm and outer 130 cm.

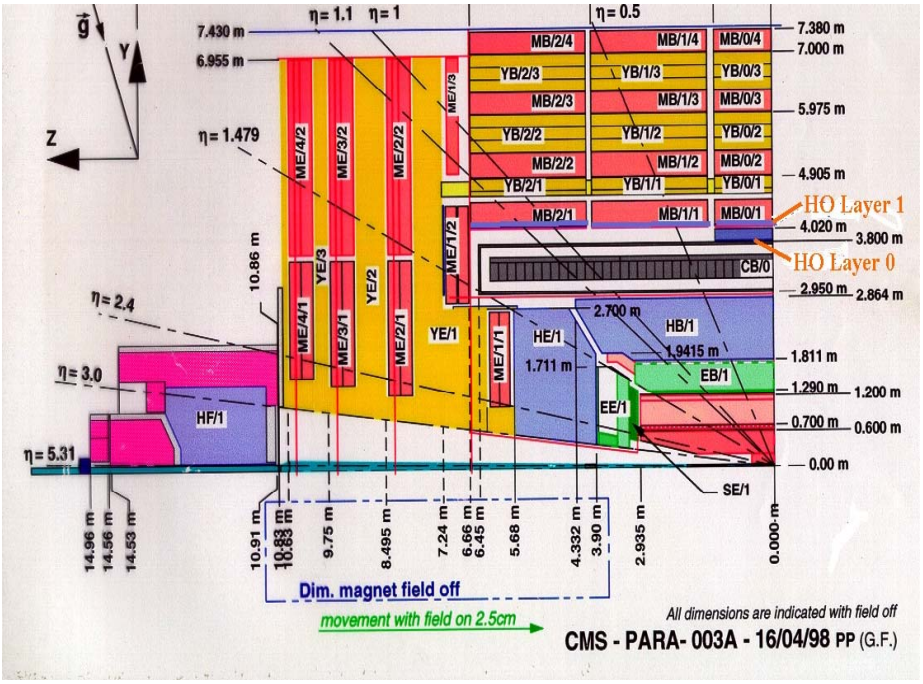

Figure 2.5: The HCAL in CMS.

2.2.4 Magnet System

The CMS magnet is made of "superconductor", through which current is passed without any resistance and creating a strong magnetic field. At ordinary temperature the strongest possible magnet has only half the strength of the CMS solenoid. The superconducting magnet for CMS has an inner diameter of 5.8 m and is 12.5 m long, a field of 4 Tesla, which is 100,000 times that of the Earth and energy stored of 2.7 GJ at full current. When a particle enters in a magnetic field it follows a curved path. If the momentum of a particle is large its path will be less curved by the magnetic field, so tracing its path gives a measure of momentum. The solenoid field serves, with the central tracker and the muon filter. As a side effect, the barrel calorimeters are protected from charged particles with low transverse momentum. Inside the magnet coil the tracker and calorimeter detectors (ECAL, HCAL) fit snugly while the muon detectors are interleaved with a 12-sided iron structure that surrounds the magnetic coils and contains and guides the field. Currently the CMS magnet provides 3.8 T field to the experiment which mainly provides the bending power for central tracker [30].

2.2.5 The Muon System

The detection of muons is important because they are expected to provide a clean signature for a wide range of physics processes especially in searches for the Higgs boson using the golden channel H $\rightarrow$ ZZ $\rightarrow 4\mu$. Muons are less ionizing particles so they deposit only a small fraction of energy in the calorimeters. Therefore the muon system is placed outside of the calorimeters [31]. The system consists of three types of gaseous particle detectors: the drift tube chambers (DT) in the barrel with $|\eta| < 1.2$, cathode strip chambers (CSC) in the endcaps with $0.9 < |\eta| < 2.4$ and resistive plate chambers (RPC) both in the barrel and the endcaps with $|\eta| < 1.6$. The CSC's chambers based on the multiwire proportional chamber (MWPC) technology with spatial resolution ranges from 75 μ to 150 μ in r-ϕ. The barrel is divided in 5 wheels, each is made of four stations of drift tubes stacks, (MB1$\sim$ MB4), interspersed among the layers of the iron yoke plates. RPC's are made by two high resistive planes (Bakelite) separated by 2 mm gas gap and a strip plane is placed between two resistive planes. It combines adequate spatial resolution and good time resolution with fast response which can differentiate muons in two consecutive bunch crossing (BX). They are placed in both endcap and barrel region.

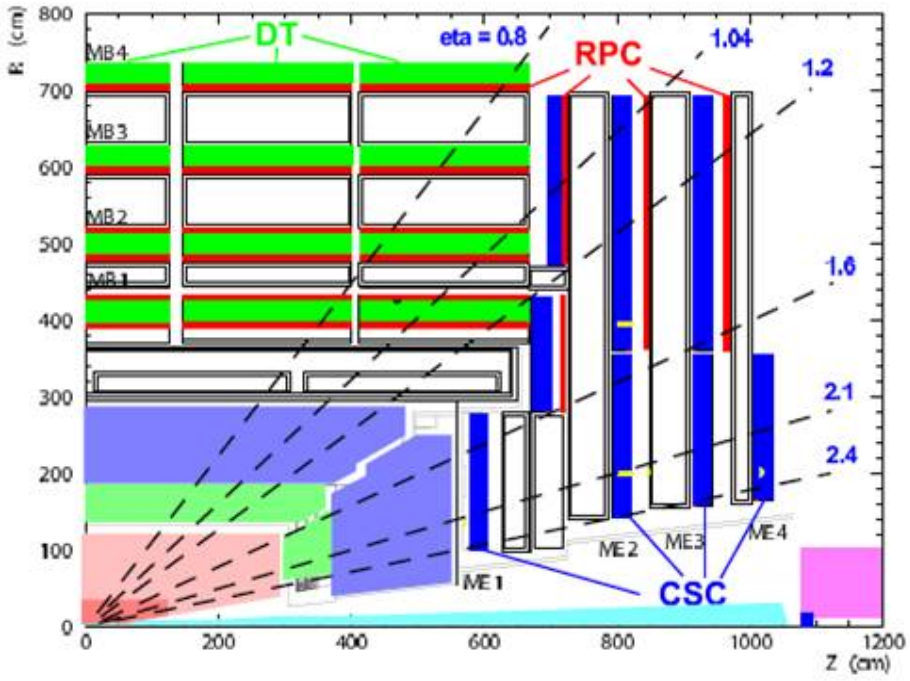

Figure 2.6: Muon System in endcap and barrel regions in CMS.

2.3 Pseudorapidity

Pseudorapidity (η) is a commonly used spatial coordinate describing the angle of a particle relative to the beam axis. Pseudo rapidity is calculated from the equation

$$\eta = -\ln(\tan\frac{1}{2}\theta) \tag{2.1}$$

where θ is the angle between the beam axis and the particle momentum **p** called polar angle [32].

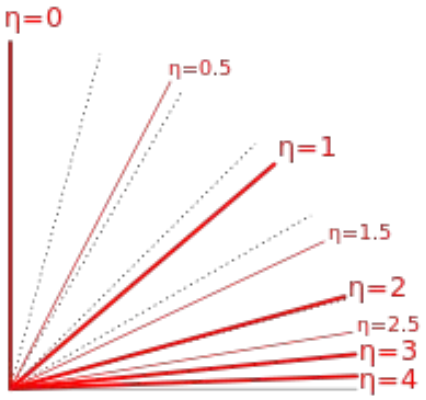

Figure 2.7: Pseudorapidity Values in 1^{st} Quadrant.

2.4 The Beam Spot

The beam spot is the luminous region in the center of CMS produced by the collisions of proton beams. The beam spot serves as an essential input for track selection, primary vertex and impact parameter computation. The beam spot parameters are very important to be measured very accurately, especially the beam spot width, which enters the computation of important observables. The beam spot also gives an excellent reference point for studying tracking performance [33].

2.5 The Trigger System in CMS

At LHC the proton bunches cross at a rate of 40M Hz. It is impossible to register the full rate of events, because the disk space and the speed of the readout electronics devices are limited. Besides that, we are not interested in all events. For example at a luminosity 10^{33} $cm^{-2}s^{-1}$, a rate of about 10^9 events with low momentum transfer, can be rejected.

Such events are called minimum bias events. Hence a trigger system is built in order to select in a short time the interesting physics events with high efficiency and reject the non interesting events by a factor 10^7. To achieve these goals the trigger system in CMS is divided in two physical steps:

- Level-1 Trigger (L1)
- High Level Trigger (HLT)

The L1 hardware trigger takes the information from the calorimeters and muon systems and is built of mostly custom-made hardware. A L1 trigger decision has to be taken for each bunch crossing within 3.2 μs. The L1 trigger task is to reduce the flux of data from 40M Hz to 100k Hz. The L1 trigger is responsible for the identification of electrons, muons, photons, jets and missing transverse energy. It consists of three main subsystems [34]:

- L1 Calorimeter Trigger
- L1 Muon Trigger
- L1 Global Trigger

The L1 Global Trigger is responsible for combining the output of the L1 Calorimeter Trigger and L1 Muon Trigger and for making the decision. The L1 Muon Trigger is actually a composed system itself: information from RPC, CSC and DT specific triggers are combined in the so called L1 Global Muon Trigger.

The High Level Trigger instead, should reduce again the L1 output rate down to the nominal rate of 100 Hz. In practice, the rate of events stored by the HLT is higher. During the 2011 data taking the output rate of the HLT was around 300 Hz in average. The HLT code runs on a farm of commercial processors and can access the full granularity of all subdetectors.

2.6 CMS Analysis Framework

CMS uses CMSSW (Compact Muon Solenoid Software) software for data analysis. It is permanently revised and extended, so one should be careful for CMSSW version. CMSSW_4_4_4 version has different structure from CMSSW_5_4_4. CMSSW is released by 'cmsrel' and the environment can be set by 'cmsenv' command [35]. The framework includes code to record data and reconstructs physical objects. A huge data is recorded by the detector so it is stored at different storage elements across the world. The Grid concept is used for this purpose. Following are the main CMSSW software elements:

- **Framework and Event Data Model (EDM):**
  The framework concept is used to modularize the software which allows the development of each component independently. It requires that every module should have a well defined event-processing functionality. The modules communicate with each other via interact through the event. The process between data and the event is described by the Event Data Model (EDM). When events pass through different modules, they can read the data from the events or add to it. The framework uses different types of modules such as Pool source, EDProducer, EDFilter, EDAnalyzer, EDLooper and Output module.

- **Simulation:**
  CMSSW software has a generator interface which incorporates different kinds of generators. Events are generated using event generator (e.g Pythia, Powheg, Madgraph) and detector simulation can also be done using generator interface.

- **Reconstruction:**
  The process in which physical quantities such as leptons or jets are constructed from the information collected by the detector is called reconstruction. In CMS there are three types of reconstruction: local reconstruction, global reconstruction and combined physics objects.

- **Analysis Tools:**
  In CMS every group has developed its own analysis tools according to their analysis requirements. Physics Analysis Toolkit (PAT) is created by Physics Analysis Groups (PAG) to be a general purpose product. It is a high-level analysis layer where the ID algorithms and reconstructed objects are included. Physics objects can be selected and cleaned in this process to eliminate the objects with poor quality. In this thesis the same PAT layer for muon, jets and missing transverse energy (MET) selection has been used.

2.7 Event Generators

Multiparticle production is the most important feature of current high-energy physics. Different event generators are used for this purpose. The Pythia generator is one of them that can be frequently used to generate such 'events'. The program is designed in such a way to generate complete events as one observe experimentally, within the bounds of our current understanding of the underlying physics [36]. The five main applications of an event generator are probably the following:

- To give physicists a feeling for the kind of events one may expect to find, and at what rates.
- As a help in the planning of a new detector, so that the detector performance is optimized.
- To use as a tool for devising the analysis strategies that should be used on real data.
- Use as a method for estimating detector acceptance corrections that have to be applied to raw data for extracting the 'true' physics signal.
- These generators provide a convenient framework within which to interpret the observed phenomena in terms of the fundamental underlying theory (usually the Standard Model).

2.7.1 POWHEG

The POWHEG (Positive Weight Hardest Emission Generator) program is used to generate events in hard collision. The program is accurate to next-to-leading order (NLO) in QCD and generates positive weighted events. It can be interface with any Shower Monte Carlo (SMC) program [37].

2.7.2 MadGraph

MadGraph is the matrix element generator, coded in the Python programming language. For a physics process of interest, MadGraph generates the amplitudes for all the relevant sub processes and produces the mappings for the integration over the phase space [38].

2.8 Particle Flow (PF) Algorithm

It is necessary to see a physical object in the whole detector not in the dedicated detectors. The particle flow algorithm (PF) is used to provide a global event description [39]. For example, a muon can be measured in the muon system as well as in the tracking system. In this way we can obtain higher reconstruction efficiency. PF algorithm has been used in this analysis.

2.9 B-tagging

The identification of b-jets is important for the discovery channels like the measurement top quark production, top quark decay, the search for Higgs boson, and many New

Physics phenomena [40]. In CMS the b-tag algorithms depend on the long life time, large momentum fraction and high mass of b-hadrons produced in b-quark jets as well as on the presence of soft leptons from semi-leptonic b-hadron decays [41].

2.9.1 B-tagging observables

- **Impact Parameter:** The Impact Parameter (IP) is the perpendicular distance between the track and the primary interaction vertex at the point of closest approach. It is calculated in 3D. IP will positive if the track is produced downstream and negative if the track is produced upstream with respect to PV.
- **Secondary vertex:** Secondary vertex is the point where the b-hadron decays.
- **Lepton:** Muon from b-hadron decay can be used to tag the b-jets.

2.9.2 B-tag algorithm

In this analysis the "Combined Secondary Vertex (CSV)" algorithm has been used. CSV algorithm provides discrimination even when no secondary vertices are found. To measure the b-tagged sample purity we use the "Mass of reconstructed charged particles coming from the Secondary Vertex" [42].

2.10 Event Shape Variables

These are the variables for studying the shape of an event whether it is spherical, planar or circular.

2.10.1 Sphericity

Sphericity is a measure of the sum of $P_{\perp}^2$ with respect to the event axis. The sphericity tensor is given as;

$$S^{\alpha\beta} = \frac{\sum_i P_i^{\alpha} P_i^{\beta}}{\sum_i |P_i|^2} \tag{2.2}$$

where α, β = x, y, z. From the diagonalization of $S^{\alpha\beta}$ we can find the three eigen values $\lambda_1 \geq \lambda_2 \geq \lambda_3$, satisfying the condition $\lambda_1 + \lambda_2 + \lambda_3 = 1$ [43]. The event's sphericity is calculated as;

$$S = \frac{3}{2}(\lambda_2 + \lambda_3), \tag{2.3}$$

so that $0 \leq S \leq 1$. For an isotropic event S ≈ 1 and a 2-jet event corresponds to S ≈ 0.

2.10.2 Aplanarity

It is the measure of transverse momentum component out of the event plane and given by;

$$A = \frac{3}{2}\lambda_3 \tag{2.4}$$

with a range constrained to $0 \leq A \leq \frac{1}{2}$. For a planar event A ≈ 0 and an isotropic event has A $\approx \frac{1}{2}$ [44]. Corresponding to the three eigenvalues λ_j, there exists eigenvectors V_i. The sphericity axis is given by V_1 while V_1 and V_2 span the plane of the sphericity event.

Two terms C and D can be defined in terms of the eigenvalues λ_1, λ_2 and λ_3.

$$C = 3(\lambda_1\lambda_2 + \lambda_1\lambda_3 + \lambda_2\lambda_3) \tag{2.5}$$

$$D = 27\lambda_1\lambda_2\lambda_3 \tag{2.6}$$

Typically C is used to measure the 3-jet structure and vanish for perfect 2-jet event while D measures the 4-jet event and vanish for a planar event.

2.10.3 Circularity

Circularity is a measure of energy spread after the collision. It is given by the relation;

$$C = 2\frac{min(\lambda_1, \lambda_2)}{\lambda_1 + \lambda_2} \tag{2.7}$$

2.11 Pile-up

In LHC the proton beams are circulated in closed packed bunches. These bunches are squeezed in order to increase the probability of proton-proton collision. When this bunches cross each other, more than one proton-proton collision take place. This is known as Pile-up (PU) [45]. It was expected that there might be an average pile-up of around 25 interactions per crossing at the design luminosity of LHC. But the pile-up recorded by CMS is more than 25 [46] at instantaneous luminosity (0.7×10^{28} cm^{-2}s^{-1}) which is lower than the designed luminosity (1×10^{28} cm^{-2}s^{-1}) of LHC even though the bunch spacing is 50 ns instead of 25 ns. The high PU increases the number of hits in the tracker which results an increase in tracks. But in an event these tracks can be distinguished by the high granular and efficient Tracker. A schematic diagram of PU is shown

in Fig. 2.8.

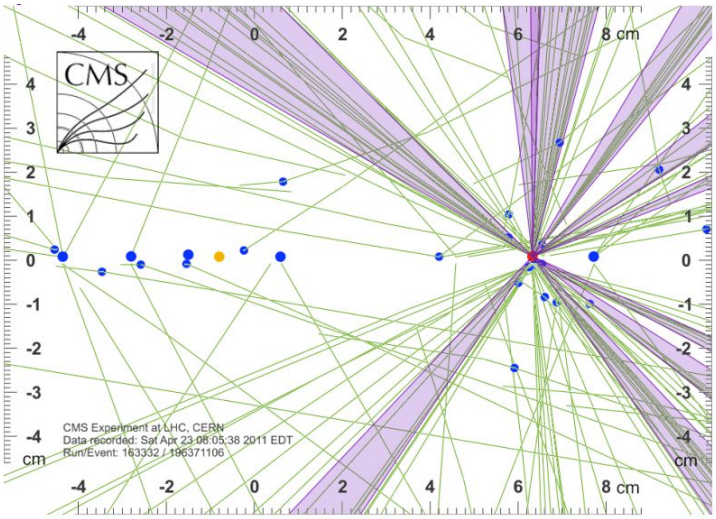

Figure 2.8: Pile-up Events.

2.12 CMS active status report 2012

Fig. 2.9 shows overall summary of CMS detector during its operation from 2010 to 2012. The performance of subdetectors is very well [47].

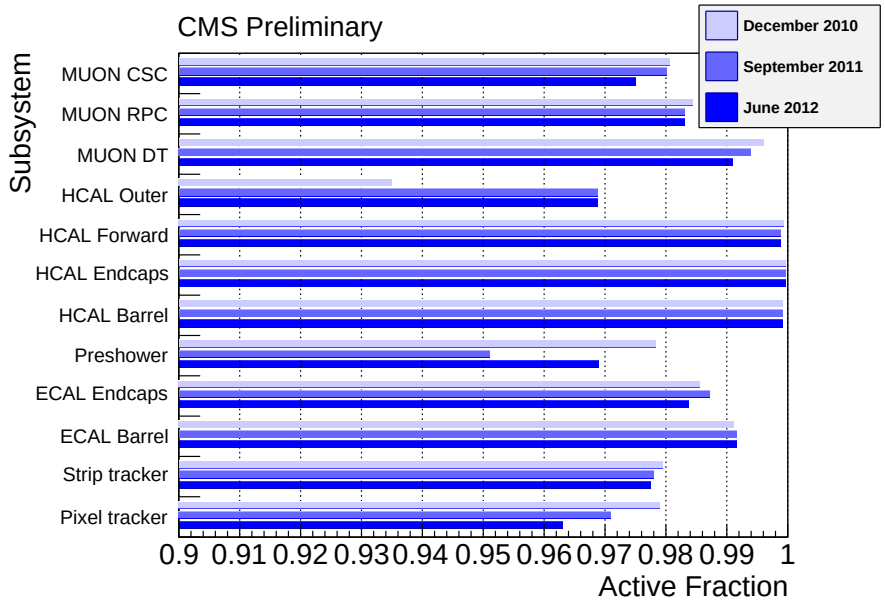

Figure 2.9: A comparison of efficiency of CMS detectors from 2010 to 2012.

Chapter 3

Data Sets and Event Selection

3.1 Monte Carlo Background Samples

This study is based on the data collected by CMS in 2011 with run number 165088-167913 and $\int \mathcal{L}dt$ = 0.959 fb^{-1} shown in table 3.2. The corresponding MC were generated using different generators, like Madgraph, Powheg and Pythia6 as shown in table 3.1. There are many processes that result in the same final state topology as signal (1 lepton, missing transverse energy and jets) [48], and thus are backgrounds to this channel. The possible main background processes that taken into account are:

- **W+Jets**
  The decay of top quark to a W boson and b-jet is exclusive (~100%). W+Jets process results in a very similar final state as the signal when W decays leptonically accompanied by additional jets. W+jets cross section is much larger than the signal; therefore a large number of events can pass through simple cut base selection. This mimics the signal and in fact constitutes dominant background to this analysis.

- **Single Top**
  This process contains a real top quark, resembles to the signal and contributes a substantial amount to the background.

- **Drell-Yan Process (Z/$\gamma^* \rightarrow ll$)**
  This process constitutes significant background when one of the lepton coming from the decay of Z boson is misidentified as jet or escape from the detector, the contributions of Drell-Yan Process to background becomes significant and mimic the signal.

- **QCD**
  The production cross section for this process is very large and practically such processes can't be generated with Monte Carlo (MC). Therefore QCD multijets events were generated with generator level filter, relevant to signal processes. For this analysis the QCD samples are generated at least one muon in final state with pT > 15 GeV.

3.2 MC samples

Monte Carlo (MC) samples [49] used for this analysis are given in table [3.1]. The data

Name	Path	σ (pb)	$\mathcal{L}$ (fb^{-1})	Notes
Signal	/TTJets_TuneZ2_7TeV-madgraph-tauola/Summer11-PU_S4_START42_V11-v1/AODSIM	157.5	23.5	NLO
W+Jets	/WJetsToLNu_TuneZ2_7TeV-madgraph-tauola/Summer11-PU_S4_START42_V11-v1/AODSIM	31314	2.597	NNLO
Z+Jets	/DYJetsToLL_TuneZ2_M-50_7TeV-madgraph-tauola/Summer11-PU_S4_START42_V11-v1/AODSIM	3048	11.9	NNLO
t s-channel	/T_TuneZ2_s-channel_7TeV-powheg-tauola/Summer11-PU_S4_START42_V11-v1/AODSIM	3.19	81.49	NNLO
t t-channel	/T_TuneZ2_t-channel_7TeV-powheg-tauola/Summer11-PU_S4_START42_V11-v1/AODSIM	41.92	93.03	NNLO
t tw-channel	/T_TuneZ2_tW-channel-DR_7TeV-powheg-tauola/Summer11-PU_S4_START42_V11-v1/AODSIM	7.87	103.48	NNLO
$\bar{t}$ s-channel	/Tbar_TuneZ2_s-channel_7TeV-powheg-tauola/Summer11-PU_S4_START42_V11-v1/AODSIM	1.44	95.819	NNLO
$\bar{t}$ t-channel	/Tbar_TuneZ2_t-channel_7TeV-powheg-tauola/Summer11-PU_S4_START42_V11-v1/AODSIM	22.65	85.864	NNLO
$\bar{t}$ tw-channel	/Tbar_TuneZ2_tW-channel-DR_7TeV-powheg-tauola/Summer11-PU_S4_START42_V11-v1/AODSIM	7.87	102.92	NNLO
QCD MuEnriched pT > 15	/QCD_Pt-20_MuEnrichedPt-15_TuneZ2_7TeV-pythia6/Summer11-PU_S4_START42_V11-v1/AODSIM	84679.3	0.296	LO

Table 3.1: Monte Carlo samples with cross sections, luminosity and the perturbative order of calculations.

set and corresponding JSON file [50] used in this analysis are given in table [3.2].

Run No	Data Set	$\mathcal{L}$ (fb^{-1})	JSON file
165088-167913	/SingleMu/Run2011A-PromptReco-v4/AOD	0.959	PromptReco, July6

Table 3.2: Data set used in this analysis, the range of run numbers, corresponding luminosity and JSON file.

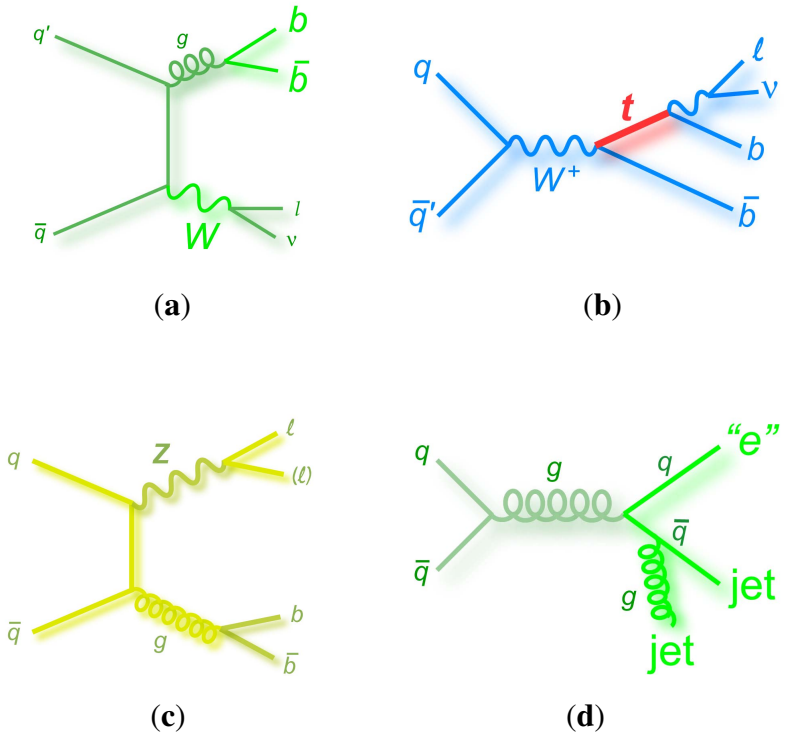

Figure 3.1: SM backgrounds to $t\bar{t}$ semiletonic decay.

3.3 Event Selection

Events containing $t\bar{t}$ decays are recognized by the decay products of the two W bosons and the two b-jets that they yield. One of the W boson decays hadronically (W→qq′) and the other leptonically (W→ μ+ $\not\!\!E_T$). This type of events with one isolated muon, $\not\!\!E_T$ (Missing Transverse Energy), four hadronic jets (two of them are tagged) are the signatures of $t\bar{t}$ events in the muon+jets channel. As mentioned in section 3.1 the main background for this analysis comes from the W+Jets, single top, Drell-Yan and QCD multijets processes. QCD multijets cross section is much larger than the signal, so we have to find a way to reduce such contamination without reducing our signal. Different cuts are applied on final objects for background reduction.

- **Trigger Selection**
  In this thesis "HLT_IsoMu_17" trigger is used that suppresses the background very well shown in table 3.6. "HLT_IsoMu_17" is the High Level Trigger (HLT) filter requires at least one isolated muon with pT ≥ 17 GeV. Data of 2011A (run no. 165088-167913) is included in this analysis so only "HLT_IsoMu_17" has been used. The trigger also supresses the large QCD background.

- **Primary Vertex**
  In the LHC the instantaneous luminosity is very high ($7 \times 10^{33}\text{cm}^{-2}\text{s}^{-1}$), which results into mulitple interactions in one single bunch crossing and objects from different interactions can be recorded in a single event. These events are known as Pile-up (PU) events, shown in Fig. 2.8. The objects in such events are mixed together and caused incorrect topology. To minimize the effect of PU, a requirement of good primary vertex is set to satisfy ndof > 4, where ndof is the number of degree of freedom corresponding to the weighted sum of number of tracks used for the construction of the primary vertex. The primary vertex must be within the range, $|z| < 24$ and $\rho < 2$ cm with respect to the interaction point.

- **Muon Isolation**
  To suppress background and extract signal, efficient cuts on muon should be applied. The muon coming from the decay of $t\bar{t}$ is expected to be well isolated from other particles in the event and have high pT because of the large mass of W boson (80 GeV). Using these two characteristics of muon we can select a muon most probably coming from the $t\bar{t}$ decay. Isolation depends upon the energy deposit or momentum by muon in the isolation cone with a cone radius $\triangle R \equiv \sqrt{(\triangle\eta)^2 + (\triangle\phi)^2}$. $\triangle\eta$ and $\triangle\phi$ are the differences in pseudorapidity and in azimuthal angle between the selected muon and the i^{th} track or calorimeter cell, respectively. In this analysis, the cone radius 0.3 has been used [51]. The combined relative isolation "RelIso" (denoted by I^{μ}_{rel}) has been widely used to select isolated leptons (muon); defined as

$$I^{\mu}_{rel} \equiv \frac{I_{trk} + I_{ecal} + I_{hcal}}{P^{\mu}_{T}} \tag{3.1}$$

  where P^{μ}_{T} is the transverse momentum of the selected muon in the l^{th} track. The isolation variables are

$$I_{trk} \equiv \sum_{i \neq l, \triangle R < 0.3} P^{track}_{T,i}, I_{ecal} \equiv \sum_{i, \triangle R < 0.3} E^{ecal}_{T,i}, I_{hcal} \equiv \sum_{i, \triangle R < 0.3} E^{hcal}_{T,i} \tag{3.2}$$

  I_{trk} is the momentum sum of all tracks in the isolation cone from tracker. I_{ecal} and I_{hcal} are the total energy depositions in the defined isolation cone from ECAL and HCAL. An optimized value of RelIso = 0.125 is used in this analysis. In addition a pT > 20 GeV cut has been applied.

- **Jet Selection**
  In $t\bar{t}$ muon+jets channel, we have at least four jets. Two of them coming directly from decay of $t\bar{t}$ known as b-jets and the other two from the hadronic decay of W boson. Combined Secondary Vertex (CSV) algorithm has been used in this

analysis for b-tagging. Jets coming from the decay of either $t\bar{t}$ or hadronic decay of W boson expected to be high pT > 30 GeV because of high top quark and W boson masses. Taking the advantage of high pT, we select leading four jets, two of them tagged (b-jets) and two non b-jets to suppress the background. In this analysis PF (Particle Flow) jets are used.

- **Second lepton veto**
  We also have to reject the $t\bar{t}$ dileptonic decay channel because it has similar characteristics like harder jet pT spectrum and isolated leptons which can mimic the signal. The criteria of second lepton veto are applied to reject dilepton events and retain more signal events. A cut of RelIso < 0.2 is applied for loose muon requirement. The event is skipped if a second loose muon is found [52].

Step	Selection	Details
0a	HLT_IsoMu17	Require exactly one isolated Muon with pT > 17 GeV
0b	Primary vertex	True vertex, ndof ≥ 4, $\|z\|$ < 24 cm and ρ < 2 cm
0c	Event cleaning (data only)	Reduce HBHE noise
1	Exactly one isol. muon	Global Muon, Tracker Muon, pT > 20 GeV, $\|\eta\|$ < 2.1, d0 (Bsp) < 0.02 cm, no. of Tracker Hits > 10, Muon Hits > 0, relIso > 0.125, △R (η, jet) > 0.3, NHitsST > 10, no. of Matches > 1
2	loose muon veto	GlobalMuon, pT > 10 GeV, $\|\eta\|$ < 2.5, relIso < 0.2
3	electron veto	$\not{E}_T$> 15 GeV, $\|\eta\|$ < 2.5, relIso < 0.2
4a,b,c	≥1,2,3 jets	PFJets, pT > 30 GeV, $\|\eta\|$ < 2.4, jet ID
5	≥4jets	PFJets.

Table 3.3: The selection cuts applied on different objects of $t\bar{t}$ semileptonic decay.

3.4 Synchronization

The purpose of synchronization is to check whether our results are consistent with other groups working on same channel or not. For this purpose different groups across the world working on the $t\bar{t}$ semileptonic muon+jets channel using CMS data have uploaded their results on the CMS TWiki page [53] . Taking these results as a reference, we applied all the standard CMS requirements for each object and compared our results with them, our results are well matched with these references. After this matching exercise we are confident to process all the data. The synchronization has been done for signal MC, data and W+jets.

3.4.1 Synchronization for signal MC

For signal MC synchronization, first 10,000 events in "/store/mc/Summer11/TTJets_TuneZ2_7TeV-madgraph-tauola/AODSIM/PU_S4_START42_V11-v1/0000/FEEE363-8-F297-E011-AAF8-00304867BEC0.root" have been used. The last row (NCP) in table 3.5 shows the synchronization done by us which is consistent with the other groups. The remarks of these groups are given in table 3.4.

3.4.2 Synchronization for W+Jets MC

For synchronization first 10,000 events in "/store/mc/Summer11/WJetsToLNu_TuneZ2_7TeV-madgraph-tauola/AODSIM/PU_S4_START42_V11-v1/0001/FED96BE1-85-9AE011-836E-001A92971B56.root" have used. The values are shown in table 3.6.

3.4.3 Synchronization for Data

The file "/store/data/Run2011A/SingleMu/AOD/PromptReco-v6/000/172/620/92127CFF-41C0-E011-ABC2-BCAEC532971F.root" has been used for data synchronization. The values of different groups are shown in table 3.7.

Group	Remarks
SQWaT	dR for Isolation = 0.4; pfRelIso for top projections < 0.20; dZ(muVtx, PV) < 0.5
UHH	unmodified JER; FastJet on; b-tag: ≥ 2 SSVHEM; pt, eta and relIso of leptons for PF2PAT top projection: same as for loose lepton vetoes; dZ(muVtx, PV) < 0.5
UHH	with +10% JER rescaling; Fast Jet on; b-tag: ≥ 2 SSVHEM; pt, eta and relIso of leptons for PF2PAT top projection: same as for loose lepton vetoes; dZ(muVtx, PV) < 0.5
Brown	Fast Jet on; b-tag: ≥ 2 SSVHEM for 2 or more jets;
Ghent	Taus not included in jets "pfNoTau"
Ghent	Taus included in jets "pfJets". Using offline Primary Vertices in pfPileUp.
Ghent	Taus included in jets "pfJets". Using good Offline Primary Vertices in pfPileUp.
Ghent	With PU reweighting.
Ghent	No PU reweighting. +10% JER rescaling. patJetGenJetMatch uses default PAT settings, matched collection ak5GenJetsNoNu.
Ghent	No PU reweighting. +10% JER rescaling. patJetGenJetMatch uses matched collection ak5GenJets.
Brussels	dR for isolation = 0.3.
Brussels	dR = 0.4; pt, eta and relIso of leptons for PF2PAT top projection same as for loose lepton vetoes.
KIT	dR isolation cone = 0.4, pfRelIso for top projection same as for loose leptons.
KIT	with PU reweighting.
NCP	No PU reweighting, jetMuonsDRPF = 0.3.

Table 3.4: Remarks of different groups for synchronization done in table 3.5.

Group	Processed Events	Cut 0a	Cut 0b	Cut 1	Cut 2	Cut 3	Cut 4a	Cut 4b	Cut 4c	Cut 5
SQWaT	10000	1521	1521	1155	1121	1008	1006	961	749	415
UHH	10000	1521	1521	1155	1121	1008	1006	961	749	415
UHH	10000	1521	1521	1155	1121	1008	1006	958	738	13
CERN-Cornell-Brunel	10000	1521	1521	1155	1121	1008	1006	961	749	415
CERN-Cornell-Brunel	10000	1521	1521	1155	1121	1008	1006	961	749	415
Brown	10000	1521	1521	1155	1121	1008	1006	961	749	415
Ghent	10000	1521	1521	1155	1121	1008	1002	929	691	375
Ghent	10000	1521	1521	1155	1121	1008	1006	961	748	414
Ghent	10000	1521	1521	1155	1121	1008	1006	961	749	415
Ghent	10000	1545	1545	1178	1148	1028	1026	981	768	422
Ghent	10000	1521	1521	1155	1121	1008	1006	964	748	415
Ghent	10000	1521	1521	1155	1121	1008	1006	958	738	413
Brussels	10000	1521	1521	1293	1267	1133	1127	1045	778	427
Brussels	10000	1521	1521	1155	1121	1008	1006	961	749	415
KIT	10000	1521	1521	1155	1121	1008	1006	961	749	415
KIT	10000	1545	1545	1178	1148	1028	1026	981	768	423
NCP	10000	1521	1521	1144	1121	1008	1006	960	748	414

Table 3.5: Synchronization of different groups for $t\bar{t}$ muon+jets channel.

Group	Processed Events	Cut 0a	Cut 0b	Cut 1	Cut 2	Cut 3	Cut 4a	Cut 4b	Cut 4c	Cut 5
SQWaT	10000	1819	1814	1333	1333	1332	184	40	7	1
SQWaT	10000	1819	1814	1333	1333	1331	184	40	7	1
CERN-Cornell-Brunel	10000		1814	1339	1339	1338	184	40	7	1
CERN-Cornell-Brunel	10000		1814	1333	1333	1332	184	40	7	1
Brown	10000	1819	1814	1333	1333	1332	184	40	7	1
UHH	10000	1819	1814	1333	1333	1331	184	40	7	1
Ghent	10000	1819	1814	1333	1333	1332	184	40	7	1
KIT	10000	1819	1814	1333	1333	1331	184	40	7	1
Brussels	10000		1814	1333	1333	1331	184	40	7	1
NCP	10000	1819	1814	1333	1333	1331	184	40	7	1

Table 3.6: Synchronization for W+Jets of different groups. Our results (NCP) are matching well at different levels of cut flow.

Group	Processed Events	Cut 0a	Cut 0b	Cut 0c	Cut 1	Cut 2	Cut 3	Cut 4a	Cut 4b	Cut 4c	Cut 5
UHH	32767	22308	22283	22278	7275	7028	7016	1171	250	47	10
Ghent				22278	7275	7028	7017	1171	250	47	10
KIT	32767	22308	22283	22278	7275	7028	7016	1171	250	47	10
KIT	32767	22308	22283	22278	7275	7028	7017	1171	250	47	10
SQWaT	32767	32759	22303		7275	7028	7016	1171	250	47	10
Brussels				22278	7276	7029	7017	1171	250	47	10
NCP	32767	22308	22286	22281	7277	7028	7017	1171	250	47	10

Table 3.7: Synchronization for Data of different groups. Our results (NCP) are matching well.

3.5 Luminosity

Luminosity of Monti Carlo (MC) can be calculated using the relation $\mathcal{L} = N\sigma$, where $\mathcal{L}$ is the luminosity, N is the number of events and σ is the cross section. These values are shown in table 3.1. For real data the luminosity can be calculated from JSON (Java Script Object Notation) file of the successful jobs [54] using "`lumiCalc2.py`". The following command has been used to calculate the luminosity of real data for this thesis. The result is shown in table 3.8.

"`lumiCalc2.py recorded -i lumiSummary.json --hltpath "HLT_IsoMu17_v*"`".

Total		959.11 (/pb)	
HLT Path	Selected LS	Recorded	Effective
HLT_IsoMu17_v10	167	4.481 (/pb)	4.481 (/pb)
HLT_IsoMu17_v11	11730	254.904 (/pb)	254.835 (/pb)
HLT_IsoMu17_v8	9381	144.378 (/pb)	144.378 (/pb)
HLT_IsoMu17_v9	25337	555.347 (/pb)	554.786 (/pb)

Table 3.8: Luminosity calculated for data 2011A.

3.6 HDECAY

HDECAY is a FORTRAN code program, which calculates the decay widths and branching ratios of SM Higgs boson and of the neutral and charged Higgs particles of the MSSM [55]. It works just like a calculator and calculates the numerical values. Table [3.9] shows the decay width and Branching Ratios (BR) of top quark in $t \to bW^+$ and $t \to bH^+$.

PDG		Width		
6		1.37656261	top decays	
BR	NDA	ID1	ID2	DECAY
0.980297410	2	5	24	BR (t → b W^+)
0.0197025899	2	5	37	BR (t → b H^+)

Table 3.9: Branching ratios (BR) and decay width of top quark. It has been calculated using HDECAY program.

3.7 A real $t\bar{t}$ event

Fig. 3.2 shows a real $t\bar{t}$ event in 2011 data. The final objects are four jets, one muon and missing transverse energy.

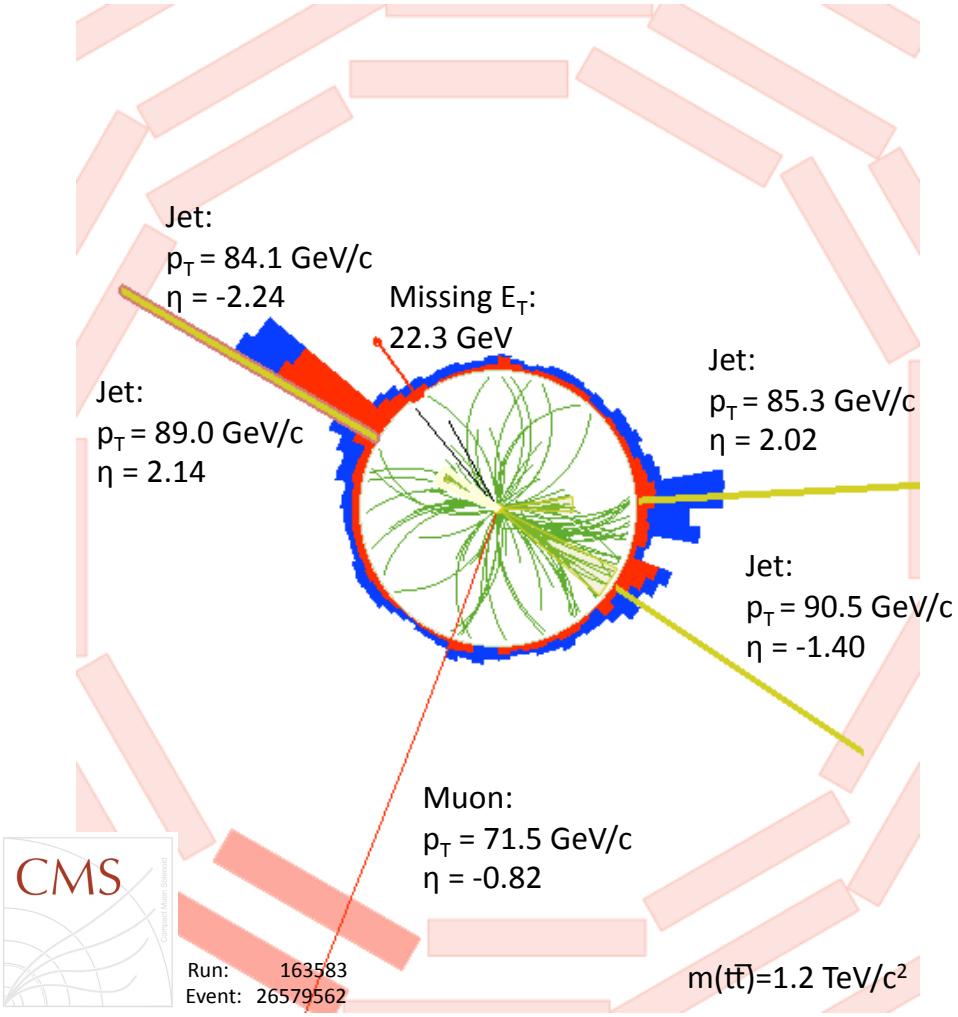

Figure 3.2: Shows a real $t\bar{t}$ event in 2011 data.

Chapter 4

Results and Discussion

4.1 Work Summary

The data used in this analysis corresponds to $\int \mathcal{L}dt = 0.959$ fb^{-1} with run number 165088-167913 collected by CMS experiment in 2011. In $t\bar{t}$ semileptonic decay one top quark decays hadronically while the other one leptonically (depends on W boson decay). Final objects of this decay channel are selected from which parameters of W boson and top quark is studied. In all the histograms signal and background MC are stacked and overlapped with data. Leading four jets, one muon and one neutrino are selected in the final state of $t\bar{t}$ decay. Two jets are identified as b-jets using Combined Secondary Vertex (CSV) algorithm and the other two are non b-jets. The two non b-jets are combined to reconstruct hadronic W boson. Using minimum angle condition, hadronic W boson is combined to one of the b-jet to reconstruct hadronic top quark. For leptonic top, muon and muon neutrino are combined to form leptonic W boson. The b-jet that form minimum angle with leptonic W is combined to leptonic W boson to reconstruct leptonic top quark. Kinematics of these objects are discussed in the following section.

4.2 Plots description

Important parameters such as transverse momentum pT, where $pT = \sqrt{P_x^2 + P_y^2}$, pseudorapidity (Sec. 2.3), azimuthal angle (ϕ) and mass are plotted. Higher transverse momentum shows that mass of the decay particle is large while pseudorapidity gives information about the direction of particle relative to beam axis. Particles with smaller pseudorapidity have larger momentum and vice versa. The dominant background contribution is coming from W+jets shown in green color in all plots. Signal MC, Z+jets, QCD and single top background are shown in red, blue, yellow and orange colors respectively. Background due to single top decay is relatively small.

4.2.1 Kinematic distribution of inclusive jets

In Fig. 4.1a, b, c and d, η, mass, ϕ and pT are plotted respectively for all jets produced in pp collision at CMS. Fig. 4.1d shows cut on pT > 30 GeV is applied given in table 3.3 which reduces most of the background. Data and MC are matching very well which shows efficient performance of the detector.

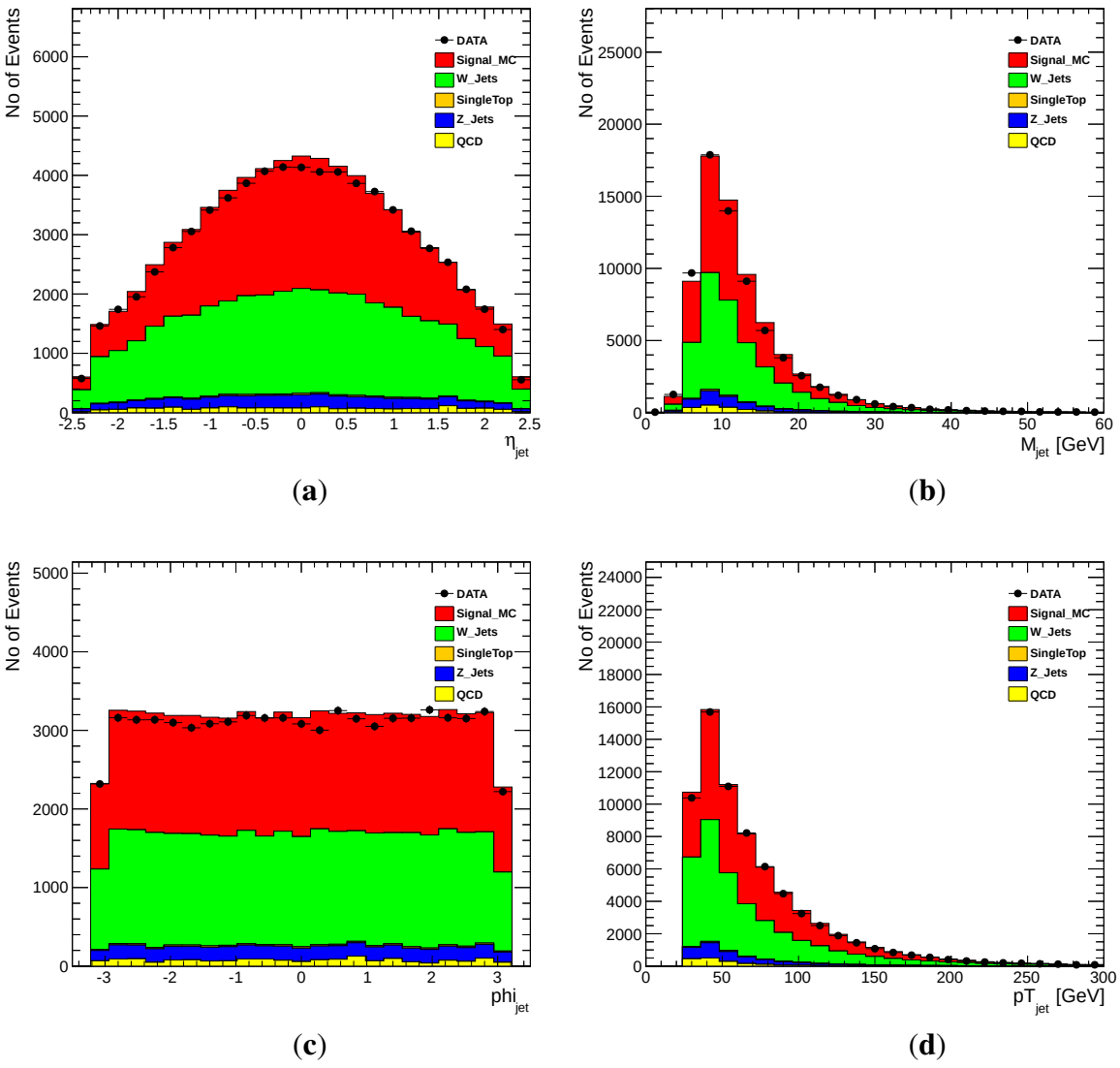

Figure 4.1: Distributions of all jets in pp collision. (a): pseudorapidity (η) of jets. (b): mass of jets. (c): distribution of azimuthal angle (ϕ) of jets. (d): transverse momentum (pT) of jets.

4.2.2 Distribution of four leading jets pT

Fig. 4.2a, b, c and d shows pT distribution of four leading jets in descending order. In Fig. 4.2a the highest pT jet is plotted with peak around 80 GeV which is higher than others. In this analysis only muon enriched QCD background is included so a mismatched in low pT region is visible. Data and MC are matching well especially in the high pT region where QCD contribution is minimal. Better agreement between data and MC is expected by properly estimating QCD background from data which will be studied as a part of my PhD dissertation.

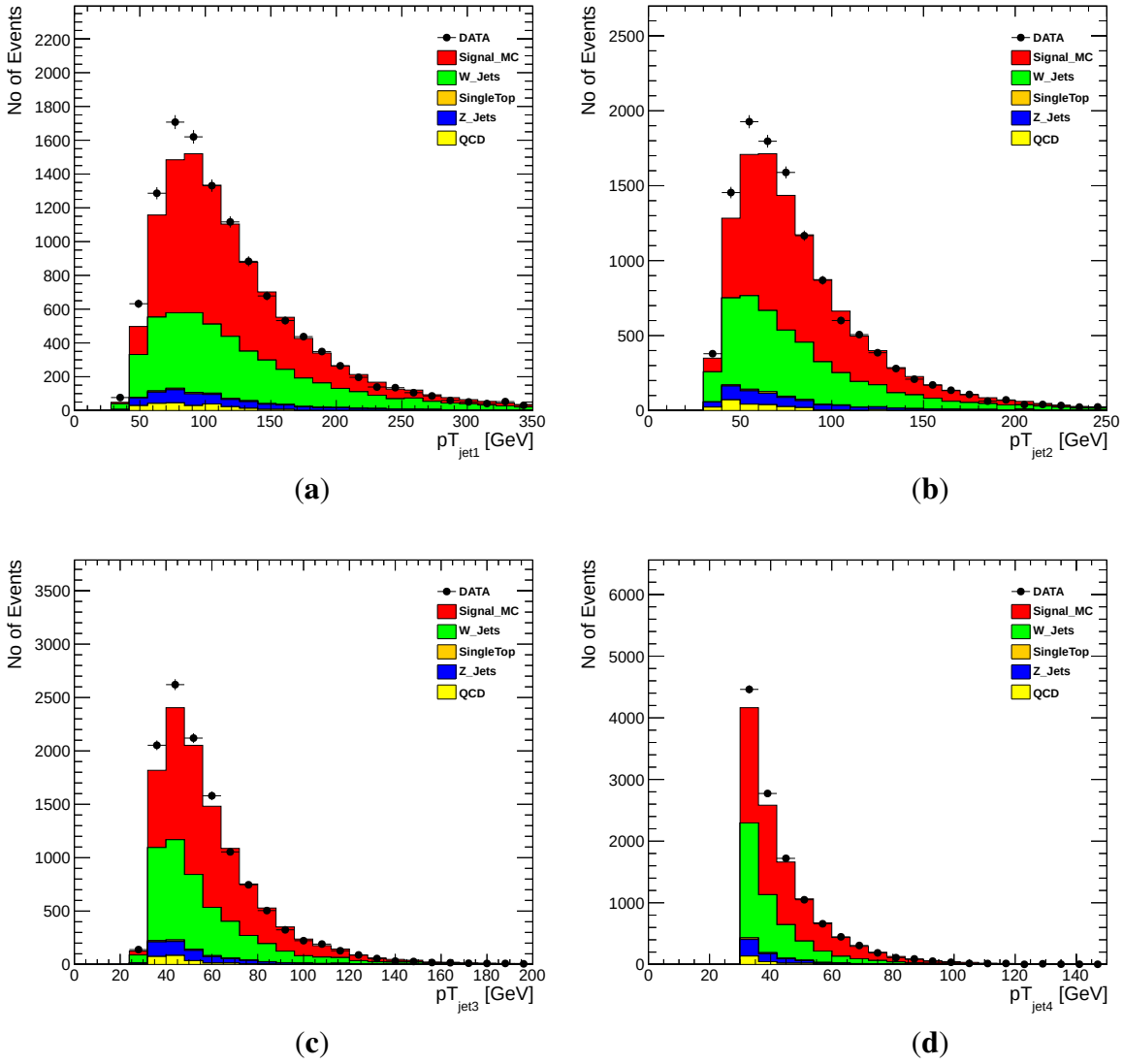

Figure 4.2: Distributions of transverse momentum (pT) of four leading jets (highest transverse momentum jets). (a): pT of leading jet. (b): pT of 2^{nd} jet. (c): pT of 3^{rd} jet. (d): pT of 4^{th} jet.

4.2.3 Pseudorapidity distribution of leading jets

Pseudorapidity distribution of four leading jets are shown in Fig. 4.3a, b, c and d. Data and MC are matching well within the statistical error. The Pseudorapidity distribution of the lowest pT jets as shown in Fig. 4.3d is broader than the leading jet plotted in Fig. 4.3a. This shows that high pT jets populate central region of the detector.

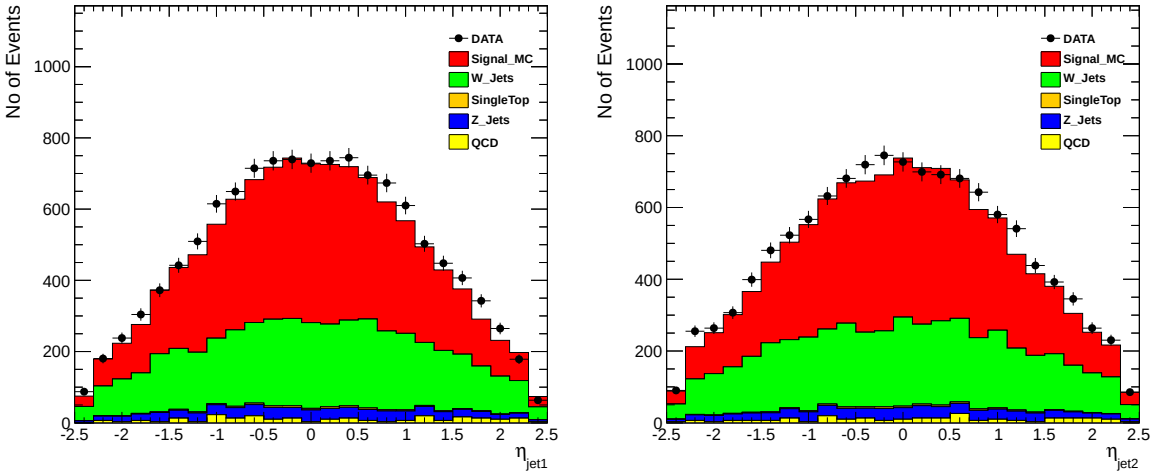

(**a**) (**b**)

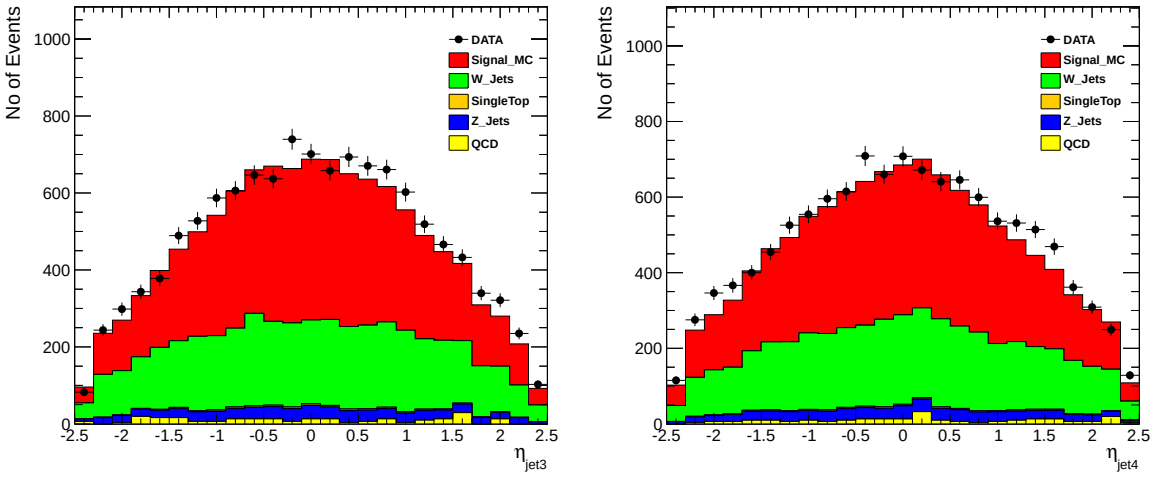

(**c**) (**d**)

Figure 4.3: Distribution of pseudorapidity (η) of four leading jets (highest transverse momentum jets). (a): η of leading jet. (b): η of 2^{nd} jet. (c): η 3^{rd} jet. (d): η of 4^{th} jet.

4.2.4 Mass distribution of leading jets

Mass distributions of the highest pT jets are plotted in Fig. 4.4a, b, c and d in descending order of their pT. In Fig. 4.4a mass of the harder jet is plotted that peaks higher than the others. A good agreement between data and MC is shown in high mass region.

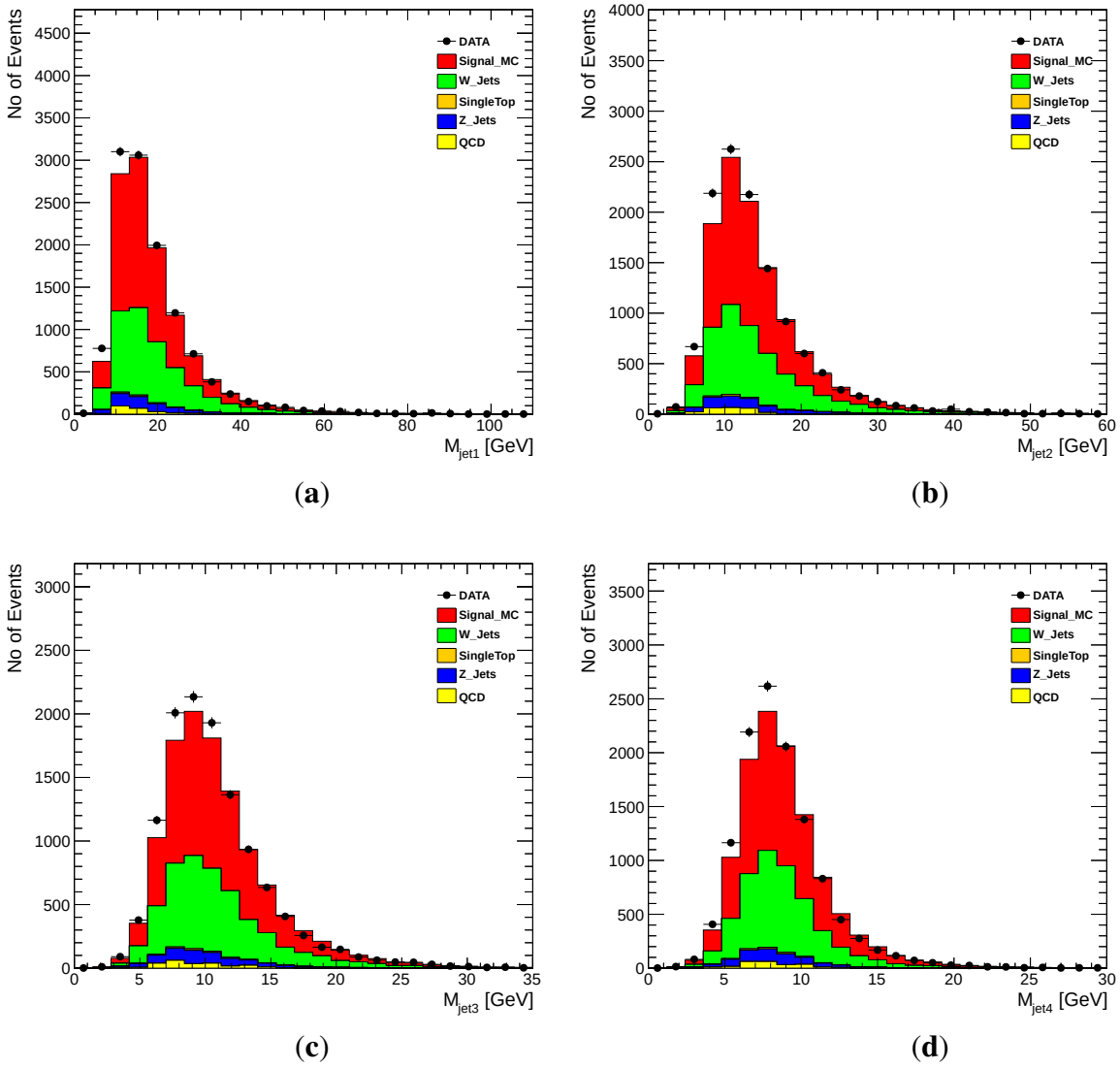

Figure 4.4: Mass distributions of four leading jets (highest transverse momentum jets). (a): mass of leading jet. (b): mass of 2^{nd} jet. (c): mass 3^{rd} jet. (d): mass of 4^{th} jet.

4.2.5 Phi distribution of leading jets

Phi distribution of four leading jets are shown in Fig. 4.5a, b, c and d. Data and MC agree well within the statistical error.

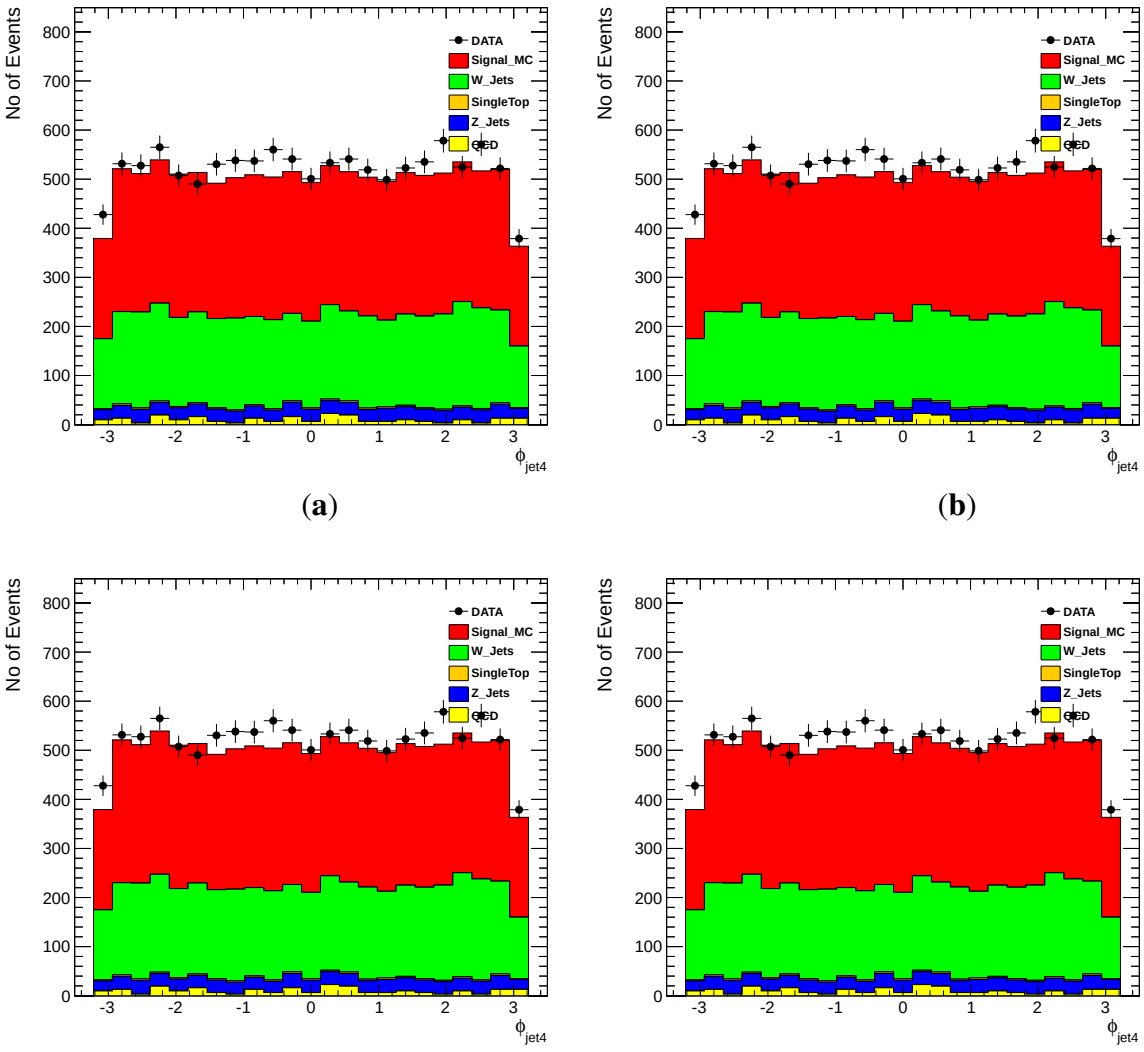

Figure 4.5: Distributions of azimuthal angle (ϕ) of four leading jets (highest transverse momentum jets). (a): phi of leading jet. (b): phi of 2^{nd} jet. (c): phi 3^{rd} jet. (d): phi of 4^{th} jet.

4.2.6 Kinematics distributions of non b-jets

To distinguish b-jets from non b-jets, CSV (with value > 0.679) discriminator cut is applied to jets. This is called b-tagging. After applying this cut, background has reduced significantly as shown in Fig. 4.6. Two higher pT non b-jets and b-jets are selected according to our requirements for the signal as discussed in section 3.3. In Fig. 4.6a and b, pT distributions of the two leading non b-jets are plotted. In Fig. 4.6c and d, η for the leading non b-jets are plotted.

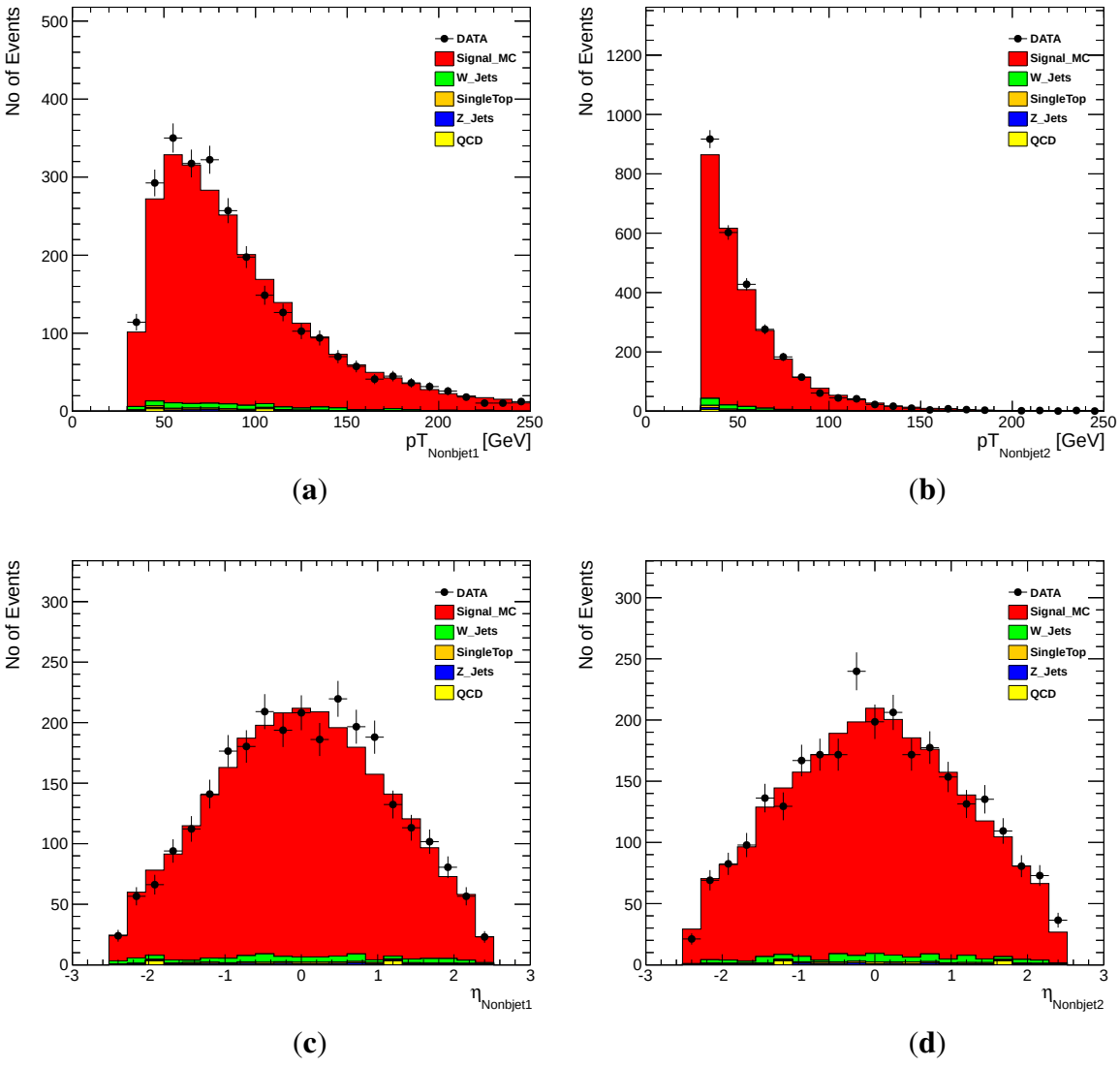

Figure 4.6: Distribution of non b-jets in $t\bar{t}$ decay. (a): transverse momentum of leading non b-jet. (b): transverse momentum of 2^{nd} non b-jet. (c): pseudorapidity (η) of leading non b-jet. (d): pseudorapidity (η) of 2^{nd} non b-jet.

4.2.7 Kinematics distributions of b-jets

In Fig. 4.7a and b, pT for b-jets are plotted in descending order. Comparing with Fig. 4.6a and b the peaks have larger values that show high pT of b-jets compare with non b-jets. In Fig. 4.7c and d, η for b-jets are plotted.

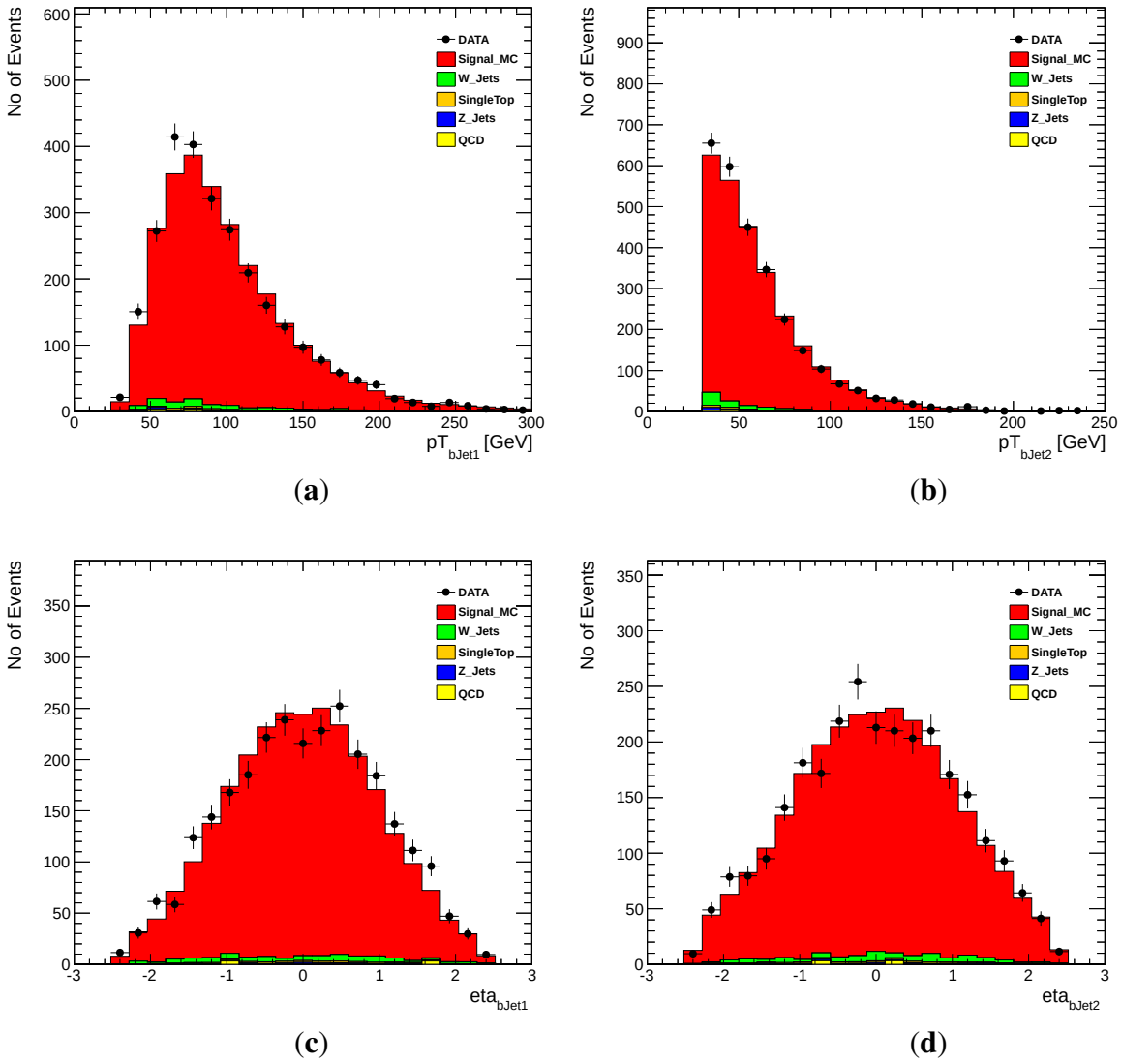

Figure 4.7: Distribution of b-jets. (a): transverse momentum of leading b-jet. (b): transverse momentum of 2^{nd} b-jet. (c): pseudorapidity (η) of leading b-jet. (d): pseudorapidity (η) of 2^{nd} b-jet.

4.2.8 Combined Secondary Vertex (CSV) distribution

Fig. 4.8a and b show ϕ distribution of two b-jets. In Fig. 4.8c, CSV discriminator is plotted. The distribution shows that at CSV > 0.679 the dominant background (W+jets) reduces significantly because W boson decay to b-jets is very rare. In the region where CSV $\leq$ 0.679, W+jets has large contribution because W boson mostly decays into light jets (non b-jets). In Fig. 4.8d Track Counting High Efficiency (TCHE) b-jet discriminator is plotted. In region above 3.30 the W+jets contribution is very rare and vice versa. In this analysis only CSV algorithm has been used.

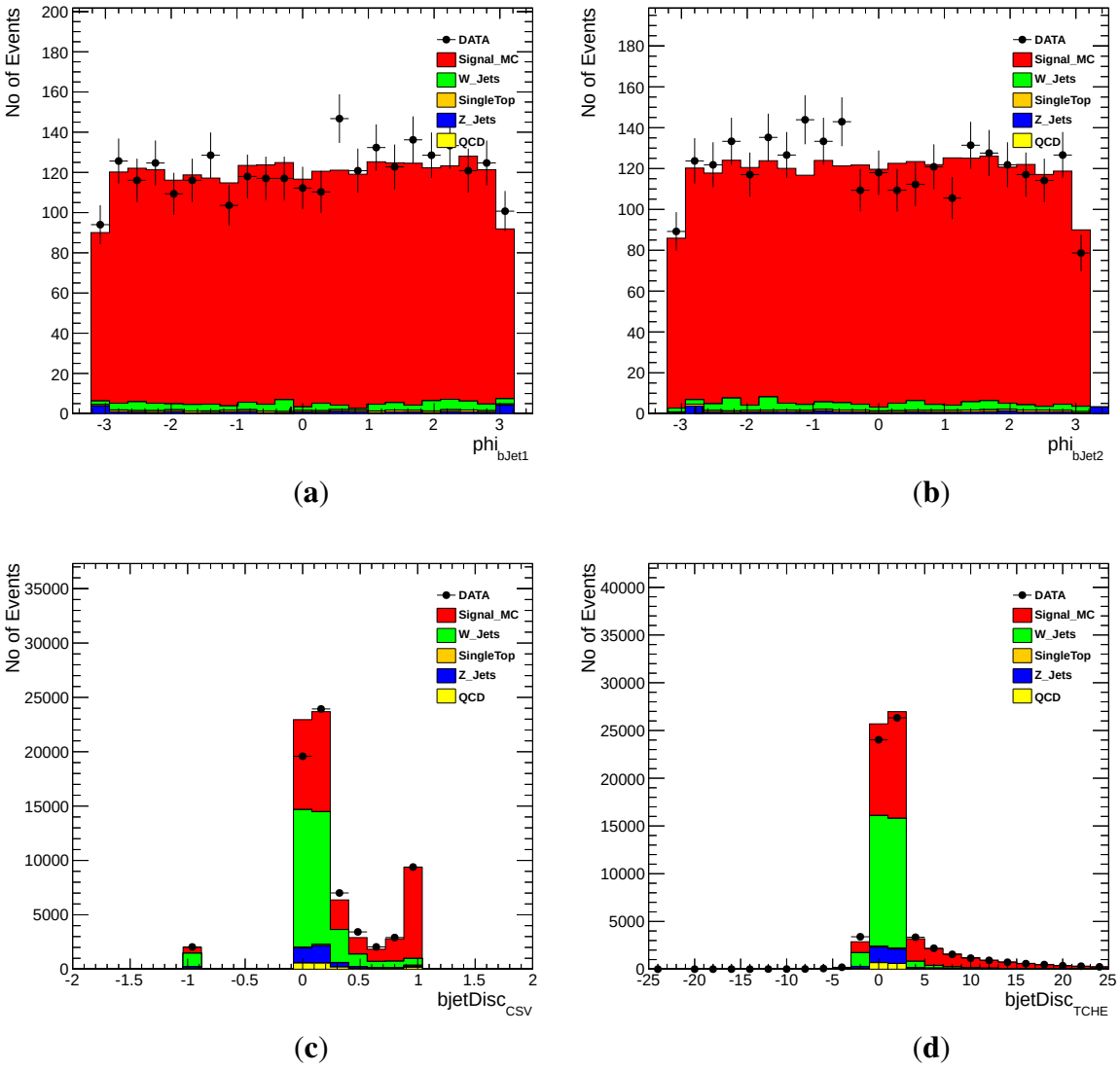

Figure 4.8: (a): phi (ϕ) distribution of leading b-jet. (b): phi (ϕ) distribution of 2^{nd} b-jet. (c): combined secondary vertex (CSV) discriminator used for b-tagging. (d): track counting high efficiency (TCHE) b-jet discriminator.

4.2.9 Hadronic W boson

After b-tagging, two jets are selected as b-jets and two non b-jets. The two non b-jets are combined to reconstruct hadronic W boson. In Fig. 4.9a, b, c and d, pT, η, ϕ and mass are plotted respectively for hadronic W boson. In Fig. 4.9d peak lies near 80 GeV which is the W boson mass. Agreement between data and MC is very good and contribution of background is significantly low after applying final selection.

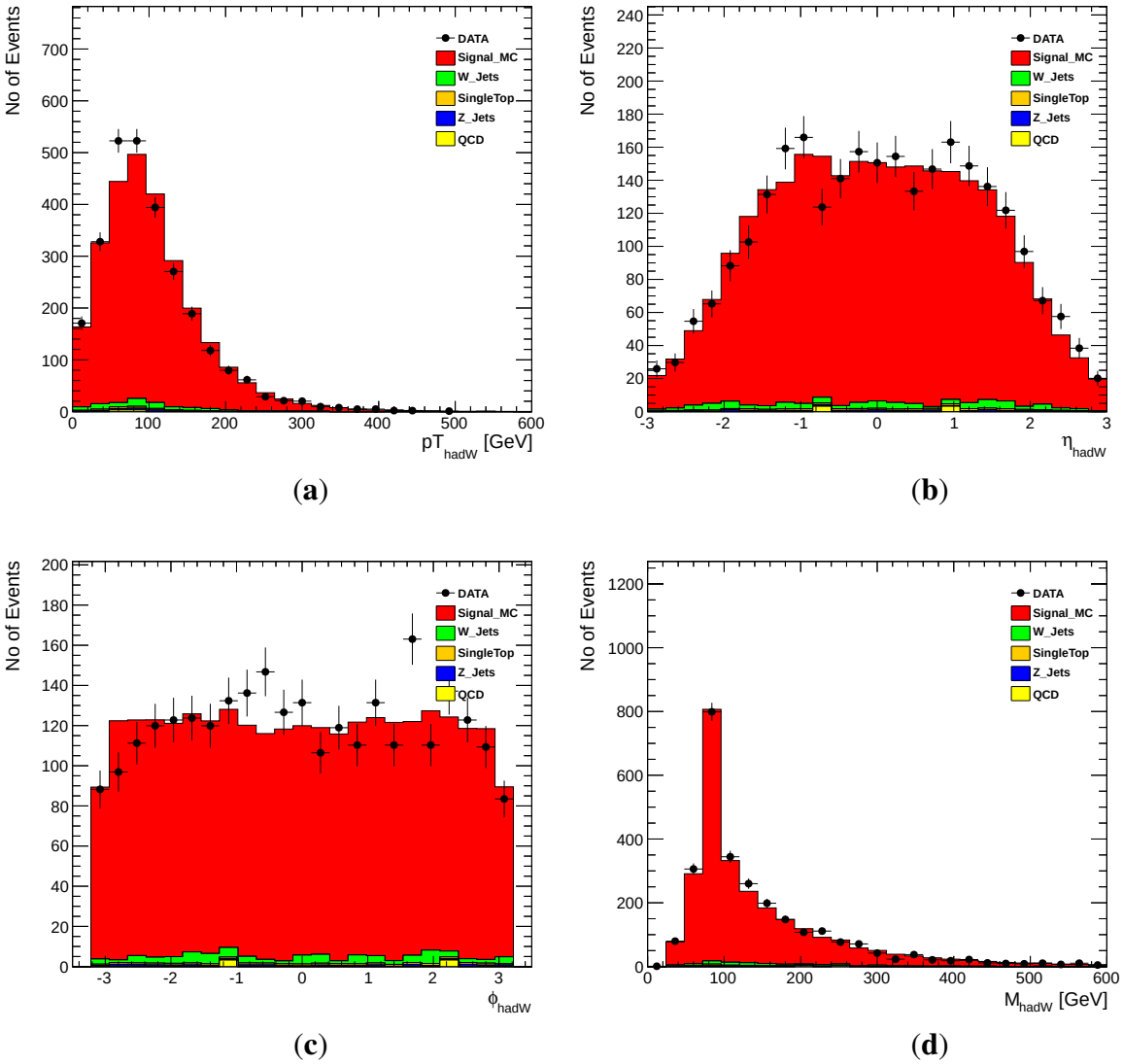

Figure 4.9: Distribution of W boson parameters reconstructed from two non b-jets. (a): transverse momentum (pT). (b): pseudorapidity (η). (c): azimuthal angle (ϕ). (d): mass of W boson.

4.2.10 Hadronic Top quark

To construct top quark from hadronic W boson, one of the b-jets that form a minimum angle with hadronic W boson is combined to reconstruct hadronic top quark. pT, η and ϕ distributions of hadronic top quark are shown in Fig. 4.10a, b and c respectively. In Fig. 4.10d mass of top quark is plotted. The peak of hadronic top mass lies around 173 GeV. A good agreement is seen between data and MC with significantly lower contribution from background.

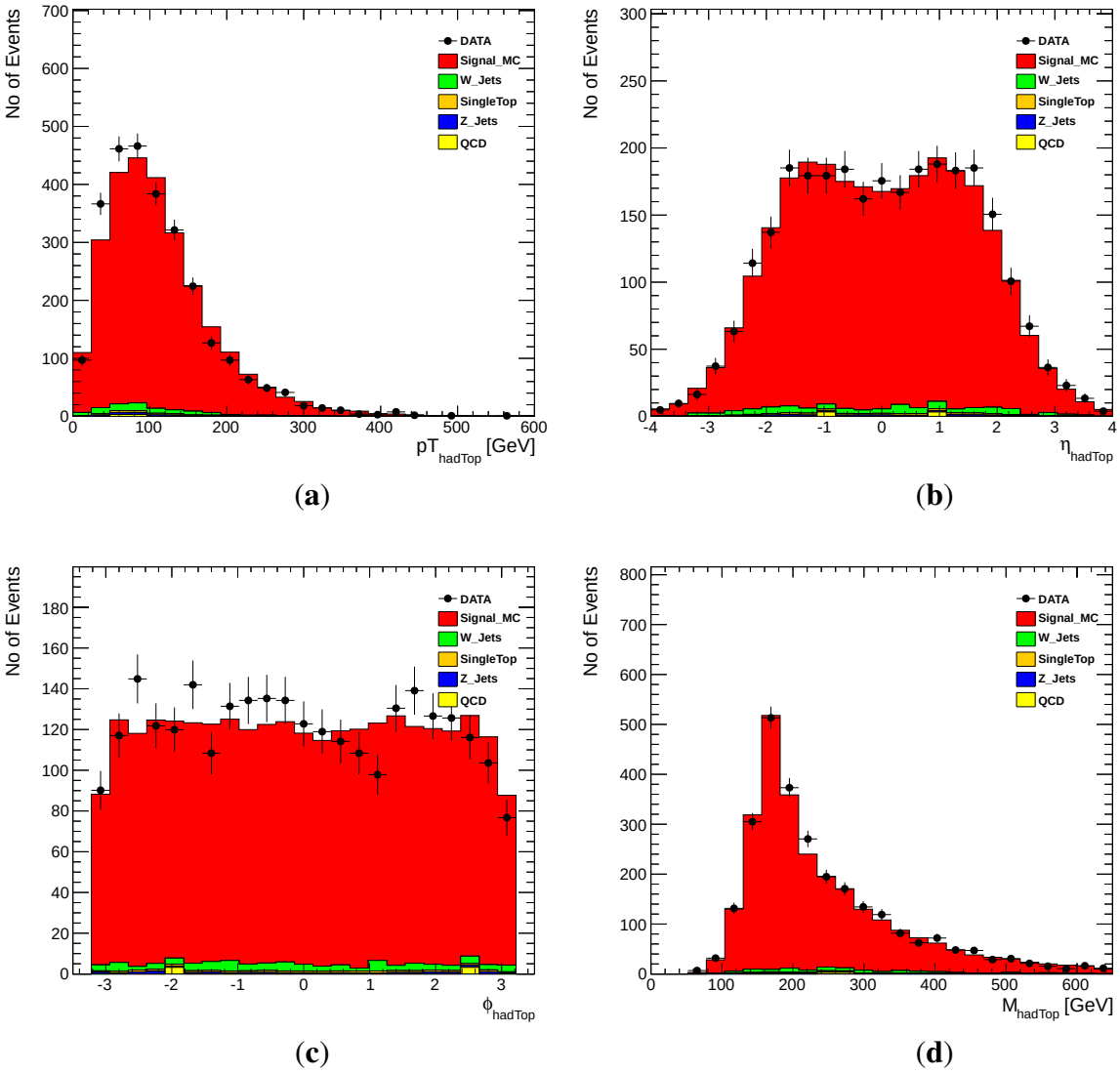

Figure 4.10: Distribution of hadronic top quark reconstructed from hadronic W boson and b-jet. (a): transverse momentum (pT). (b): pseudorapidity (η). (c): azimuthal angle (ϕ). (d): mass of top quark.

Distributions of x, y and z components of momentum for hadronic top are plotted in Fig. 4.11a, b, c respectively. The spread in z-component of momentum distribution is large as compared to x and y axis. Fig. 4.11d shows distribution of transverse energy which peaks around 150 GeV. The large value of transverse energy is a sign of boosted top quark.

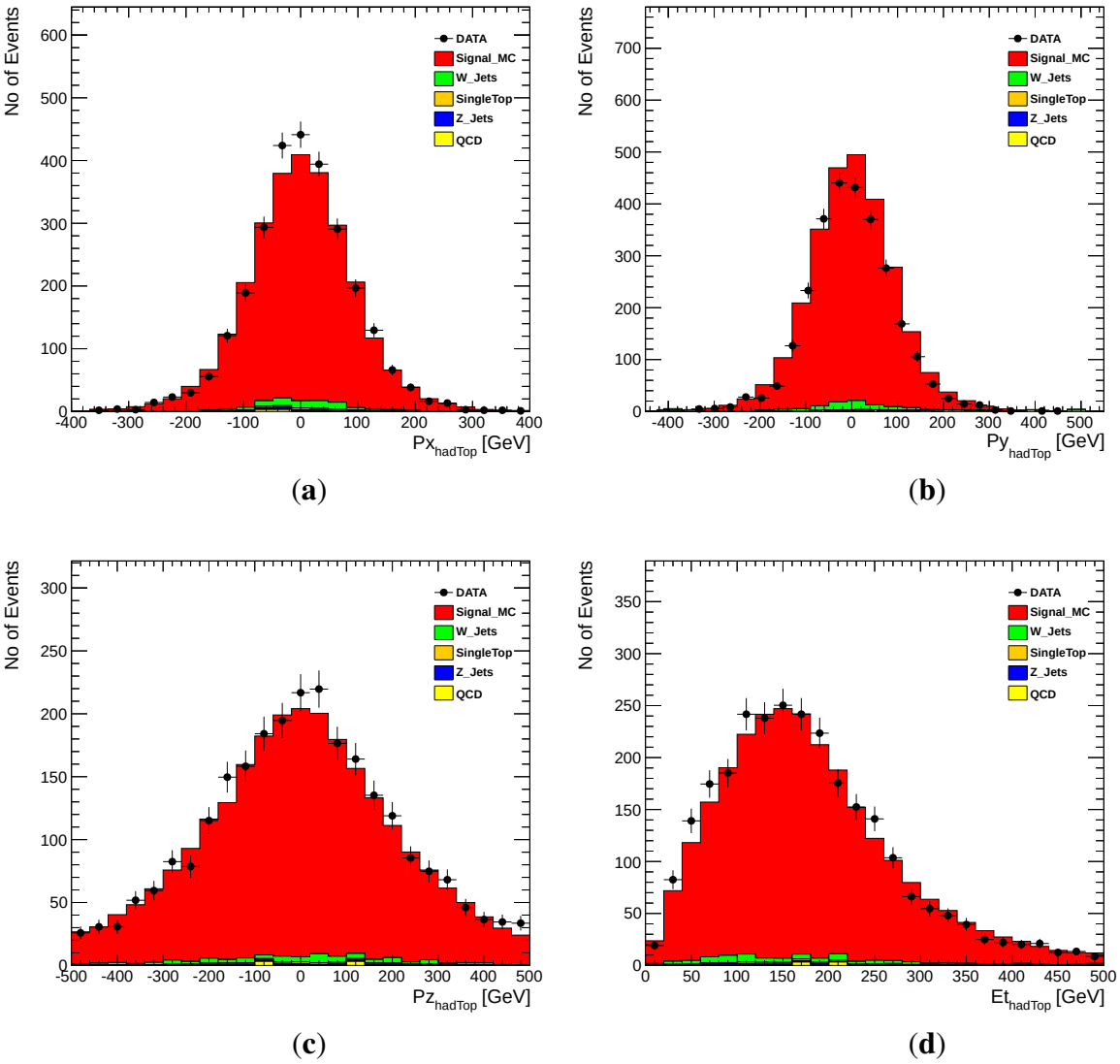

Figure 4.11: Distribution of hadronic top quark reconstructed from hadronic W boson and b-jet. (a): x-component of momentum. (b): y-component of momentum. (c): z-component of momentum. (d): the transverse energy.

4.2.11 Muon kinematics

In Fig. 4.12a, b and c, muon pT, η and ϕ are shown respectively. A cut on pT > 20 GeV has been applied as shown in Fig. 4.12a. A good agreement between data and MC is seen with small statistical error. The background contribution from W+jets is large and is shown in green color in plots. To conserve lepton number in the decay of W boson, muon has accompanied by its anti-neutrino. Due to the negligible interaction of neutrino with matter it is treated as missing transverse energy in the detector.

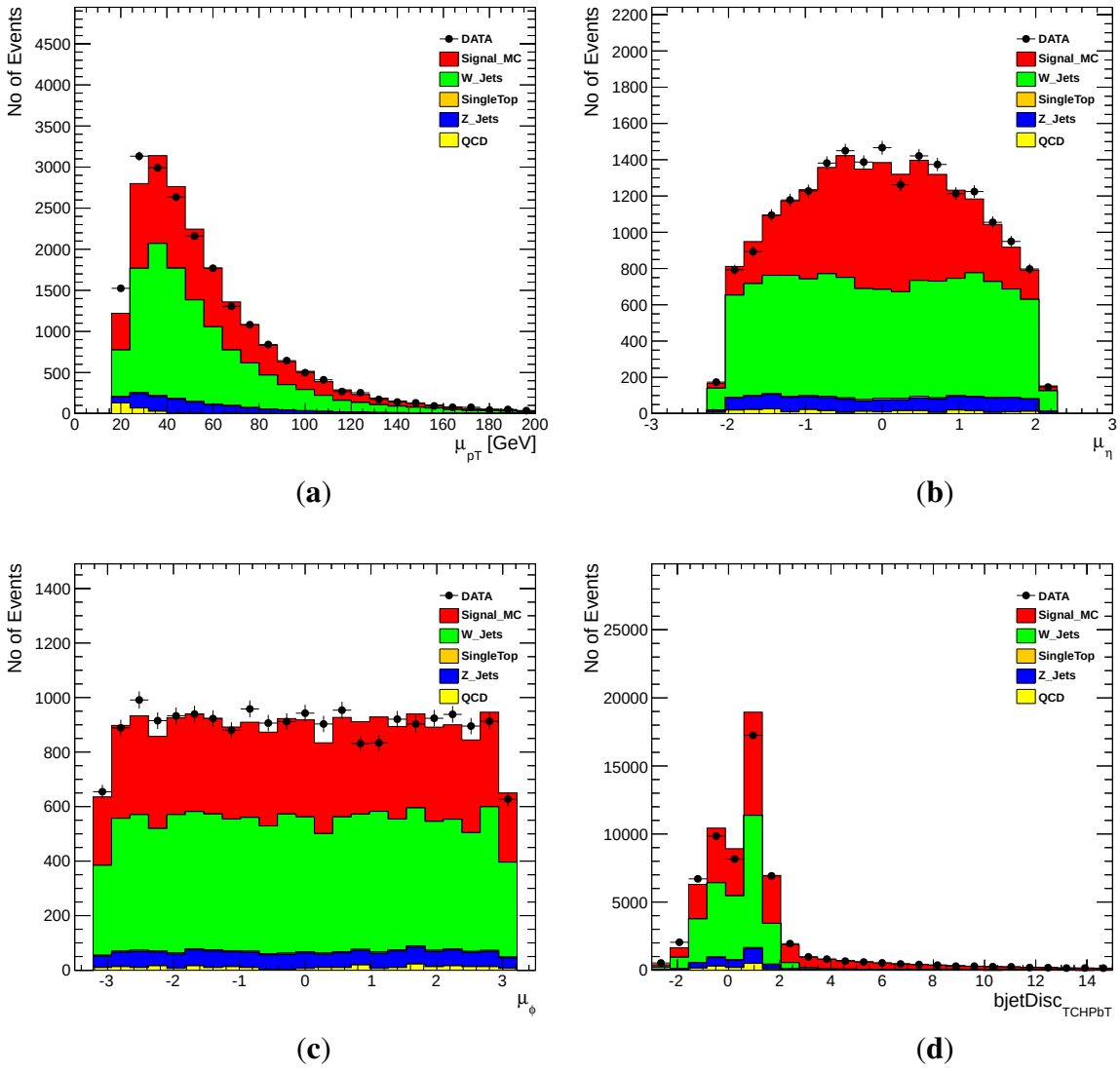

Figure 4.12: (a): Transverse momentum of the selected muon. (b): pseudorapidity (η) of the selected muon. (c): phi (ϕ) distribution of the selected muon. (d): track counting high purity b-tagging (TCHPbT) discriminator.

4.2.12 Missing Transverse Energy (MET)

MET distribution is shown in Fig. 4.13a. Maximum background contribution is from W+jets as shown in green color because most of the time W boson decay into leptons. The distribution of ϕ for MET is plotted in Fig. 4.13b. In Fig. 4.13c photon isolation is plotted. Fig. 4.13d shows the distribution of opening angle between muon and MET. Most of the time their separation is around 1.5 radians as shown by the peak value of the distribution.

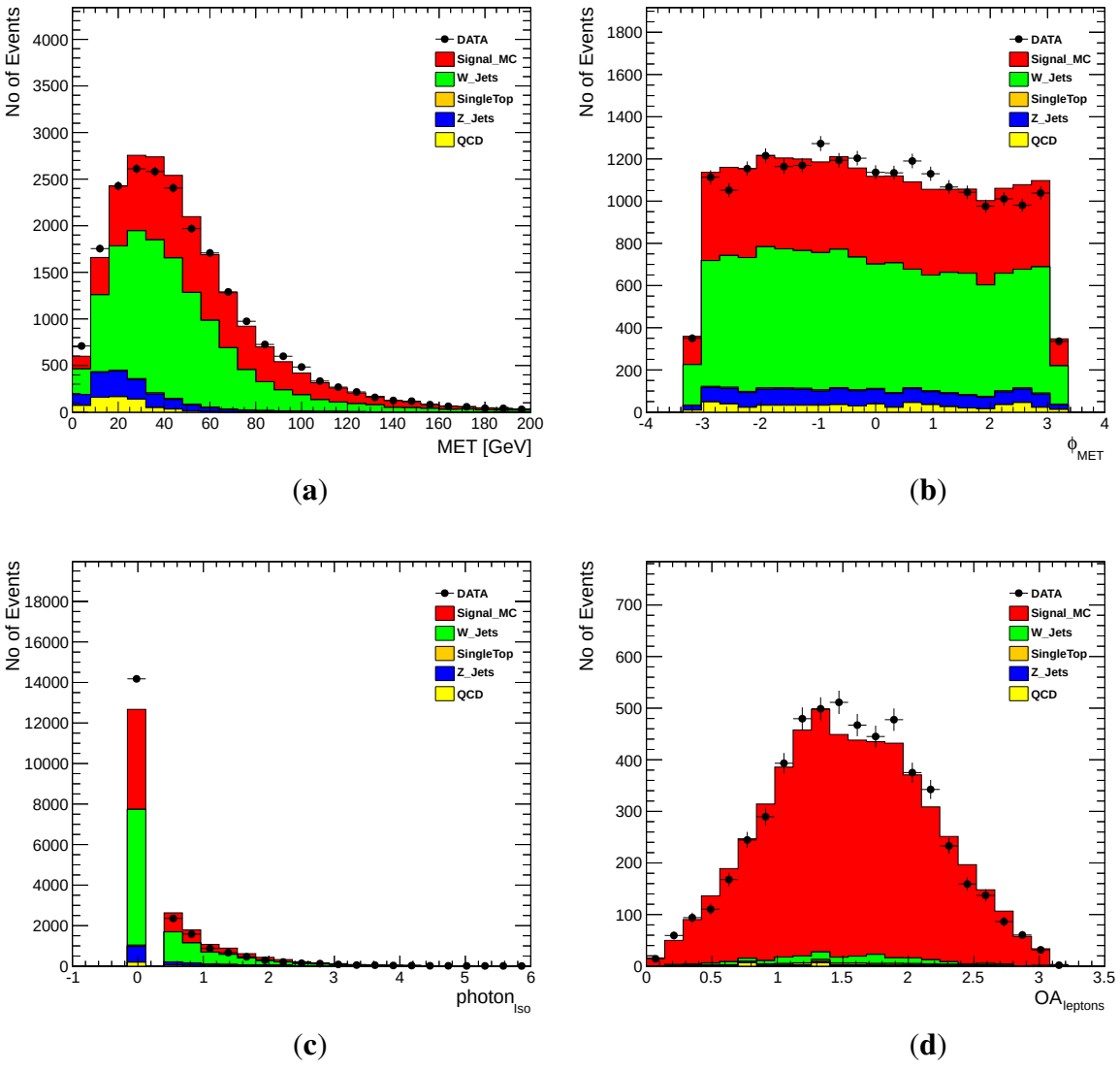

Figure 4.13: (a): Missing transverse energy (MET) distribution. (b): phi distribution of MET. (c): photon isolation. (d): opening angle between muon and MET.

4.2.13 Kinematics of leptonic W boson

Muon and its neutrino are combined to form leptonic W boson. Distributions of η, mass, transverse energy and transverse mass of leptonic W boson are plotted in Fig. 4.14a, b, c and d respectively. The η distribution has minimum spread as compared to hadronic W shown in Fig. 4.9b which shows that most of the time leptonic W has transverse direction to the beam axis. Mass of the leptonic W peaks around 80 GeV. A good agreement between data and MC is observed.

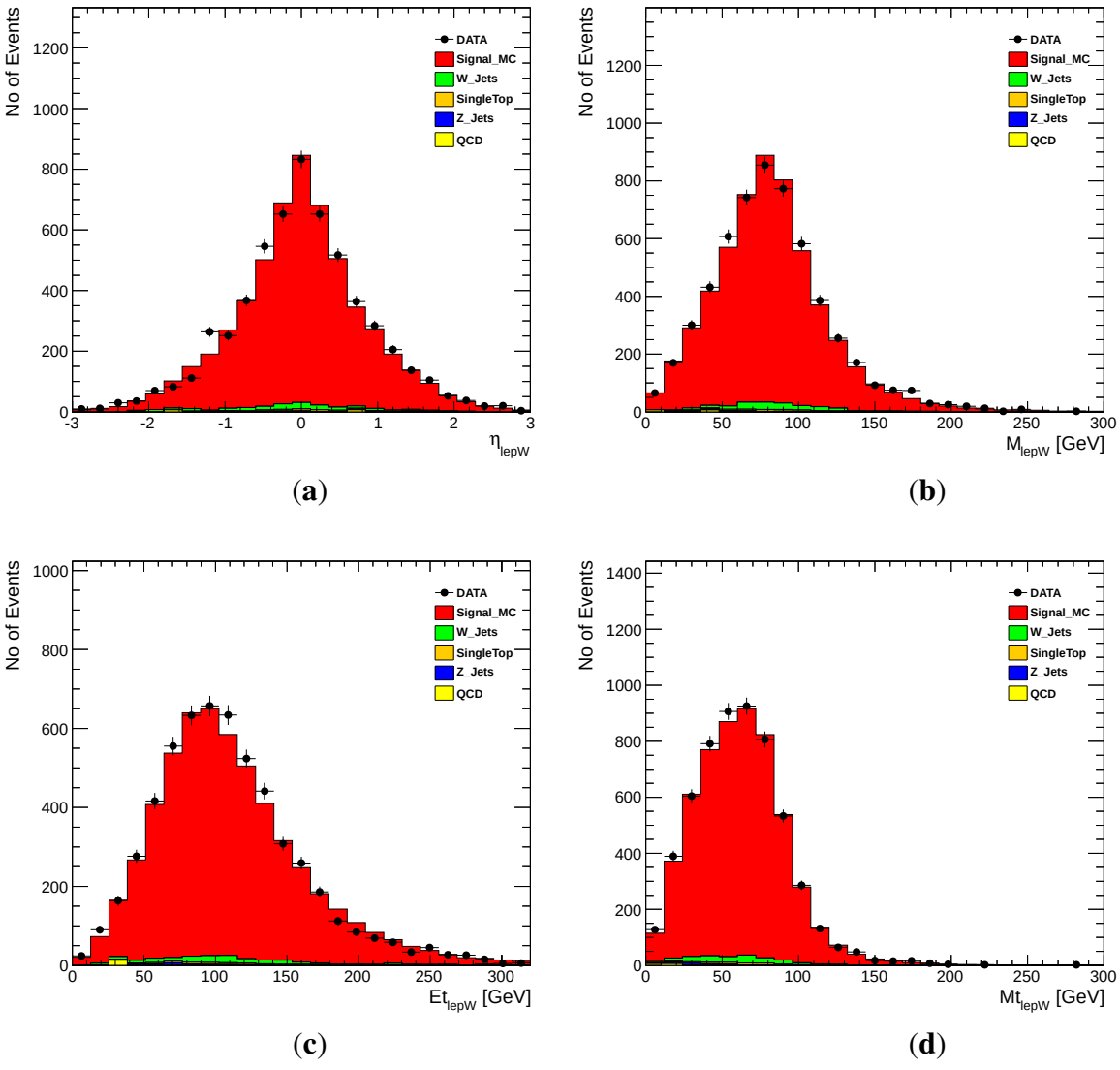

Figure 4.14: Distribution of W boson (leptonic W boson) constructed from muon and missing transverse energy (MET). (a): the pseudorapidity. (b): mass of W boson. (c): the transverse energy. (d): the transverse mass.

4.2.14 Leptonic Top quark

Top quark decay to a b-jet and W boson is inclusive. The leptonic W boson that form minimum angle with b-jets is combined to construct leptonic top quark. Kinematics of leptonic top quark are plotted in Fig. 4.15. In Fig. 4.15a, η of leptonic top shows less spread as compared to hadronic top in Fig. 4.10b because of its daughter particle namely leptonic W. Mass of leptonic top quark peaks close to 173 GeV as shown in Fig. 4.15b. A good agreement between data and MC is observed within the statistical error.

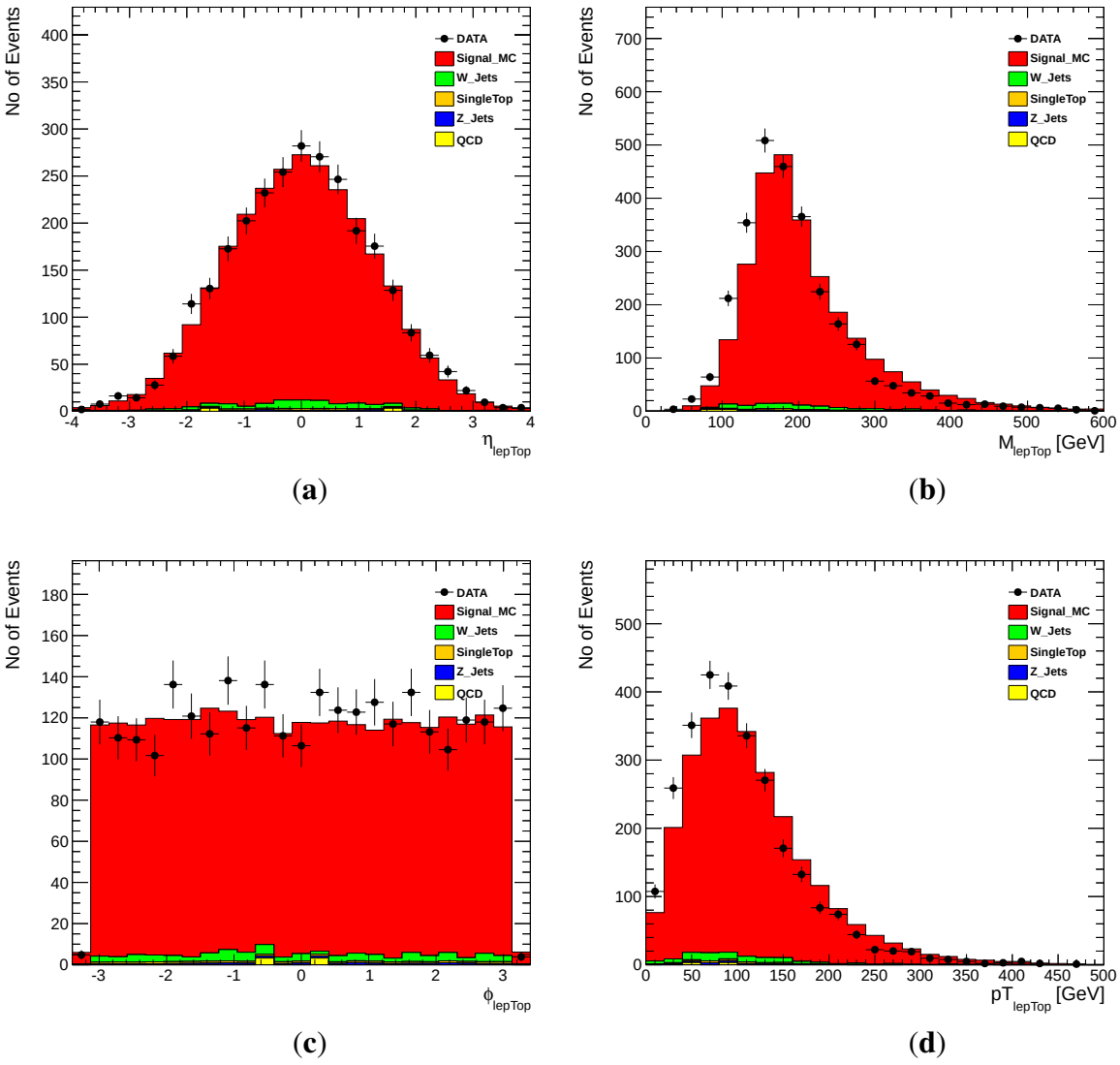

Figure 4.15: Distribution of top quark reconstructed from the leptonic W boson and b-jet (leptonic top quark). (a): the pseudorapidity. (b): the mass of leptonic top quark. (c): the phi distribution. (d): the transverse momentum.

In Fig. 4.16a, b, c and d transverse energy, transverse mass, momentum distribution along x and y axis are plotted respectively.

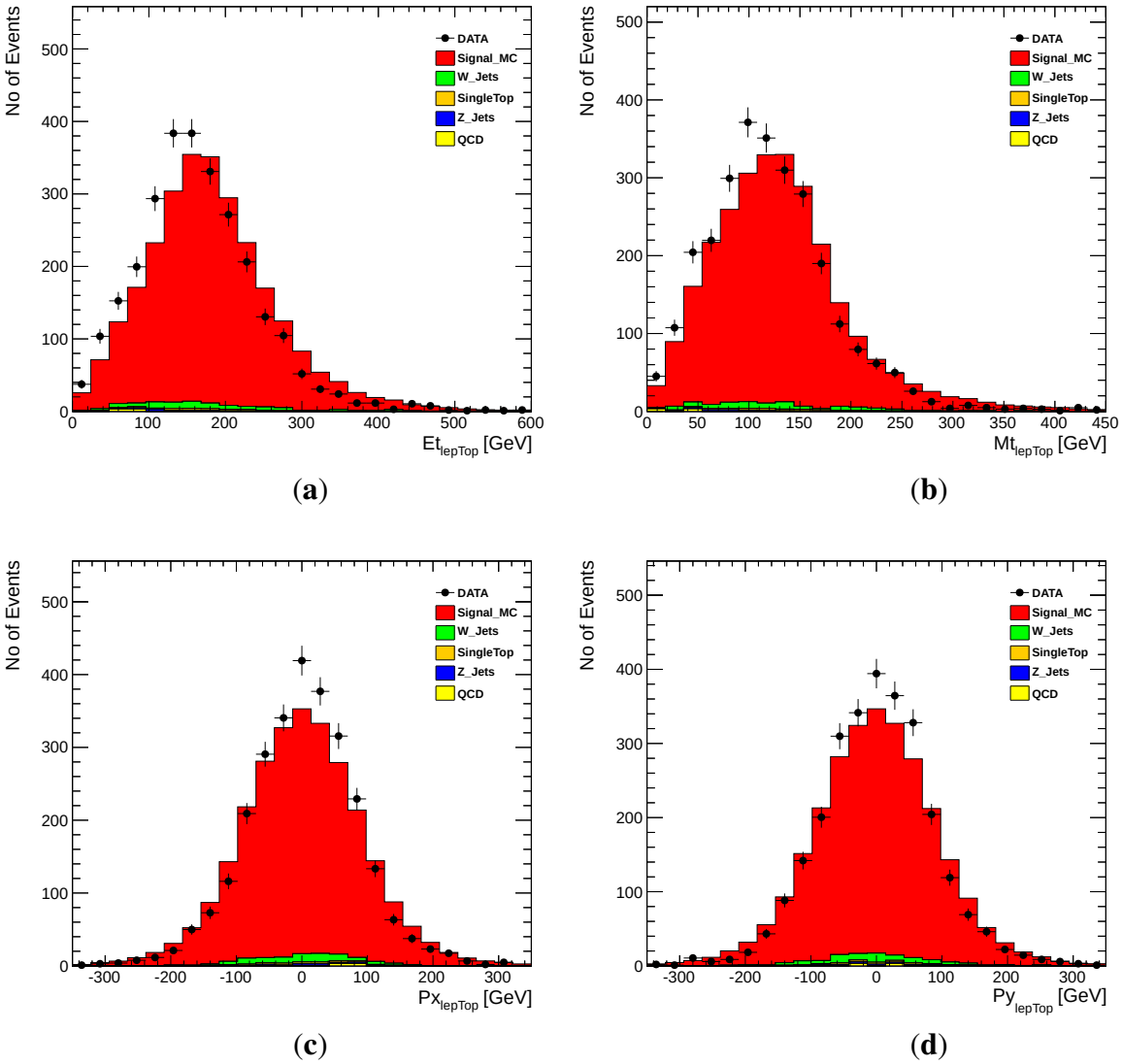

Figure 4.16: Distribution of top quark reconstructed from the leptonic W boson and b-jet (leptonic top quark). (a): the transverse energy. (b): transverse mass. (c): x component of momentum (d): y component of momentum.

In Fig. 4.17a momentum distribution along z axis is shown. It has more spread as compared to x and y axes distributions shown in Fig. 4.16c and d. Plots in Fig. 4.17b, c and d show the spatial distribution of leptonic top quark along x, y and z axis respectively. These plots show a good agreement between data and MC within the statistical error.

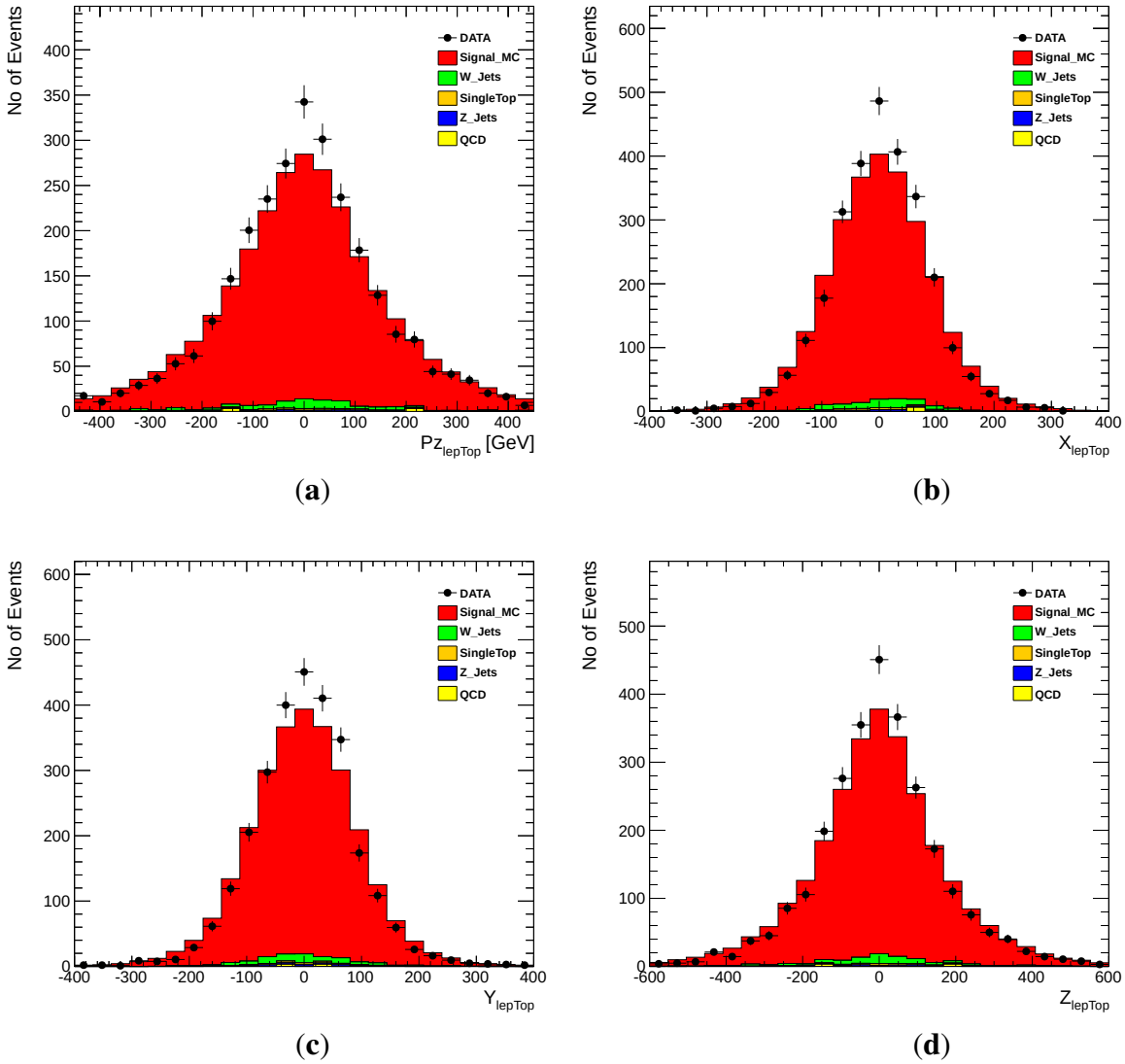

Figure 4.17: Distribution of leptonic top quark. (a): the z component of momentum. (b): x component in space. (c): y component in space. (d): z component in space.

Conclusion

The study of $t\bar{t}$ is very important because it forms background for many physical processes especially in Higgs and beyond the Standard Model searches. The results shown of this thesis have been obtained by analyzing the data recorded by CMS in 2011 (run number 165088-167913) in pp collision at a center-of-mass energy of 7 TeV, corresponding to an integrated luminosity of 0.959 fb^{-1}. Particle Flow (PF) algorithm has been used for jets reconstruction. Signal and background have been normalized with data luminosity. A good agreement has been observed between data and Monte Carlo after taking into account all backgrounds. This study compares W boson and top quark properties between data and MC using part of LHC data from 2011. Due to lack of available time and resources, we were unable to process full dataset of 2011. Through this work, we have learnt all the necessary tools required for the precise measurement of top mass. For future work, the research project will include full data from 2011 and 2012 corresponding to 5 fb^{-1} and 22 fb^{-1} respectively. Use of full data will help us to reduce the statistical error on top mass measurement. In our future work we will also estimate the systematic error of our measurement.

Bibliography

[1] David Griffiths. *Introduction to Elementary Particles*. JOHN WILEY & SONS, INC, 1987.

[2] H. Spiesberger1 M. Spira2 & P. M. Zerwas3. THE STANDARD MODEL: PHYSICAL BASIS AND SCATTERING EXPERIMENTS. *arxiv [hep-ph/0011255]*, 2000.

[3] Fayyazuddin and Riazuddin. *A modern introduction to particle physics*. World Scientific: Singapore, New Jersey, London, Hong Kong, third edition, 2011.

[4] Halliday Resnick and Walker. *Fundamentals of Physics*. WILEY, 8^{th} edition, 2007.

[5] The **DØ** Collaboration. Measurement of the W Boson Mass. *Phys. Rev.* ***D52****, 4784*, 1995.

[6] I. Bigi. CP Violation an Essential Mystery in Nature's Grand Design. *Surveys High Energ. Phys.* ***12*** *269-336*, 1998.

[7] The **CDF** Collaboration. Observation of Top Quark Production in $p\bar{p}$ Collisions with the Collider Detector at Fermilab. *Phys. Rev. Lett.* ***74*** *2626*, 1995.

[8] The **DØ** Collaboration. Search for High Mass Top Quark Production in pp Collisions at $\sqrt{s}$ = 1.8 TeV. *Phys. Rev. Lett.* ***74*** *2422*, 1995.

[9] The **CMS** Collaboration. Measurement of the Top Quark Pair Production Cross Section in $\sqrt{s}$ = 7 TeV pp Collisions using Lepton + Jets Events. *Phys. Lett.* ***B720*** *83*, 2013.

[10] C. Amsler et. al. Particle Data Group (PDG). *Phys. Lett.* ***B667****, 1*, 2008.

[11] Dhiman Chakraborty Jacobo Konigsberg & David Rainwater. Review of Top Quark Physics. *Ann. Rev. Nucl. Part. Sci.* ***53*** *301-351*, 2003.

[12] The **CMS** Collaboration. Measurement of the $t\bar{t}$ Production Cross Section in pp Collisions at $\sqrt{s}$ = 7 TeV using the Kinematic Properties of Events with Leptons and Jets. *EPJC **9** 1721*, 2011.

[13] The **CMS** Collaboration. Measurement of the single-top-quark t-channel cross section in pp collisions at $\sqrt{s}$ = 7 TeV. *JHEP **12** 035*, 2012.

[14] The **CMS** Collaboration. Measurement of the $t\bar{t}$ production cross section in all-jet final states in pp collisions at $\sqrt{s}$ = 7 TeV. *JHEP **1305** 065*, 2012.

[15] The **CDF** Collaboration. Measurement of the Top Pair Production Cross Section in the Dilepton Decay Channel in $p\bar{p}$ Collisions at $\sqrt{s}$ = 1.96 TeV. *Phys. Rev. **D82** 052002*, 2010.

[16] The **CDF** Collaboration. Measurement of the $t\bar{t}$ Production Cross Section in 2 fb^{-1} of $p\bar{p}$ Collisions at $\sqrt{s}$ = 1.96 TeV Using Lepton Plus Jets Events with Soft Muon Tagging. *Phys. Rev. **D79** 052007*, 2009.

[17] The **CDF** Collaboration. First Measurement of the Fraction of Top Quark Pair Production Through Gluon-Gluon Fusion. *Phys. Rev. **D75** 031105*, 2007.

[18] The New York Times. Physicists Find Elusive Particle Seen as Key to Universe. `http://www.nytimes.com/2012/07/05/science/cern-physicists-may-have-discovered-higgs-boson-particle.html`, 2012.

[19] The **ATLAS** Collaboration. Observation of a New Particle in the Search for the Standard Model Higgs Boson with the ATLAS Detector at the LHC. *Phys. Lett. **B716** 1-29*, 2012.

[20] The **CMS** Collaboration. Observation of a new boson at a mass of 125 GeV with the CMS experiment at the LHC. *Phys. Lett. **B716** 30*, 2012.

[21] The **CMS** Collaboration. Search for standard model Higgs boson production in association with a top quark pair in pp collisions at the LHC. *arXiv:1303. 0763. v1*, 2013.

[22] **CERN**. The Large Hadron Collider. `http://public.web.cern.ch/public/en/lhc/lhc-en.html`, 2012.

[23] Claudia-Elisabeth Wulz. The **CMS** experiment at **CERN**. doi:10. 1117/12. 620786.

[24] The **CMS** Collaboration. Detector Performance and Software. *Technical Design Report CMS 8.1*, 2006.

[25] The **CMS** Collaboration. Tracker Technical Design Report. *CERN/LHCC 98-6 CMS TDR 5*, 1998.

[26] The **CMS** Collaboration. The CMS experiment at the CERN LHC. *JINST **3** S08004*, 2008.

[27] The **CMS** Collaboration. The Electromagnetic Calorimeter Technical Design Report. *Technical Design Report CMS 4*, 2008.

[28] C. Charlot P. Busson. A METHOD FOR ELECTRON/PHOTON RECONSTRUCTION IN CMS $PbWO_4$ CRYSTAL ECAL. Technical report, CMS-TN/95-074, 1995.

[29] The **CMS** Collaboration. Missing transverse energy performance of the CMS detector. JINST **6** 09001, 2011.

[30] C-E Wulz (**CMS** Collaboration). Measurement technology for the CMS experiment. *Meas. Sci. Technol. **18** 2424*, 2007.

[31] DONALD E.GROOM et. al. MUON STOPPING POWER AND RANGE TABLES 10 MeV.100 TeV. `http://www.idealibrary.com`, 2001.

[32] The **CMS** Collaboration. Transverse momentum and pseudorapidity distributions of charged hadrons in pp collisions at $\sqrt{s}$ = 0.9 and 2.36 TeV. *JHEP **1002** 041*, 2010.

[33] Francisco Yumiceva. BeamSpot. `https://twiki.cern.ch/twiki/bin/view/CMSPublic/SWGuideFindingBeamSpot`, 2011.

[34] H. Czyrkowski et. al. RPC Based CMS Muon Trigger PROGRESS REPORT. CMS TN/93-111, 1993.

[35] **CMS** Twiki. Which CMSSW release to use. `https://twiki.cern.ch/twiki/bin/view/CMSPublic/WorkBookWhichRelease`, 2012.

[36] Torbjorn Sjostrand et. al. PYTHIA 6.4 Physics and Manual. *JHEP **0605** 026*, 2006.

[37] Stefano Frixione et. al. The POWHEG-hvq manual. *arXiv: 0707. 3081*, 2009.

[38] Johan Alwall et. al. MadGraph/MadEvent. *JHEP **0709** 028*, 2007.

[39] The **CMS** Collaboration. Particle Flow Event Reconstruction in CMS and Performance for Jets, Taus, and Missing Transverse Energy. CMS PAS PFT-09-001, 2009.

[40] The **CMS** Collaboration. b-Jet Identification in the CMS Experiment. CMS PAS BTV-11-004, 2012.

[41] Heavy Flavor Averaging Group (HFAG). Averages of b-hadron and c-hadron Properties at the End of 2007. *arXiv:0808.1297 [hep-ex]*, 2008.

[42] The **CMS** Collaboration. Measurement of the $t\bar{t}$ Production Cross Section in pp Collisions at 7 TeV in Lepton + Jets Events Using b-quark Jet Identification. *Phys. Rev.* ***D84****, 092004*, 2011.

[43] M.L. Mangano et. al. ALPGEN, a generator for hard multiparton processes in hadronic collisions. *JHEP* ***0307*** *001*, 2003.

[44] Torbjorn Sjostrand. PYTHIA 6.4 Physics and Manual. *JHEP* ***0605*** *026*, 2006.

[45] Nature. LHC prepares for data pile-up. `http://www.nature.com/news/lhc-prepares-for-data-pile-up-1.10596`, 2012.

[46] CMS.web. Reconstructing a multitude of particle tracks within CMS. `http://cms.web.cern.ch/news/reconstructing-multitude-particle-tracks-within-cms`, 2012.

[47] CMS Twiki. Active Channels in 2012. `https://twiki.cern.ch/twiki/bin/rdiff/CMSPublic/ActiveChannelsSummary`, 2012.

[48] Geng-Yuan-Jeng. *Measurement of the Top Quark Pair Production Cross Section in pp Collisions at a Center-of-Mass Energy of 7 TeV with the CMS Experiment at the LHC*. PhD thesis, UNIVERSITY OF CALIFORNIA RIVERSIDE, 2011.

[49] CMS Twiki. MC samples. `https://twiki.cern.ch/twiki/bin/view/CMS/TWikiTop2011DataMCTrig`, 2011.

[50] CMS. JSON files for 2011. `https://cms-service-dqm.web.cern.ch/cms-service-dqm/CAF/certification/Collisions11/7TeV/Prompt`, 2011.

[51] CMS Twiki. Top PAG Reference Selections for 2011. `https://twiki.cern.ch/twiki/bin/viewauth/CMS/TWikiTopRefEventSel2011`, 2011.

[52] The **CMS** Collaboration. Measurement of the top quark mass in the lepton+jets channel using the ideogram method with 5.0 fb^{-1}. Analysis Note, 2011.

[53] CMS Twiki. Synchronization for 2011 Reference Selection for the ttbar→ Muon+Jets Channel. `https://twiki.cern.ch/twiki/bin/viewauth/CMS/TopRefSelSynch2011mujets`, 2011.

[54] CMS Twiki. The official CMS Luminosity Calculation. `https://twiki.cern.ch/twiki/bin/viewauth/CMS/LumiCalc`, 2012.

[55] M.Spira et. al. HDECAY. *Comput. Phys. Commun. 108 56-74*, 1998.